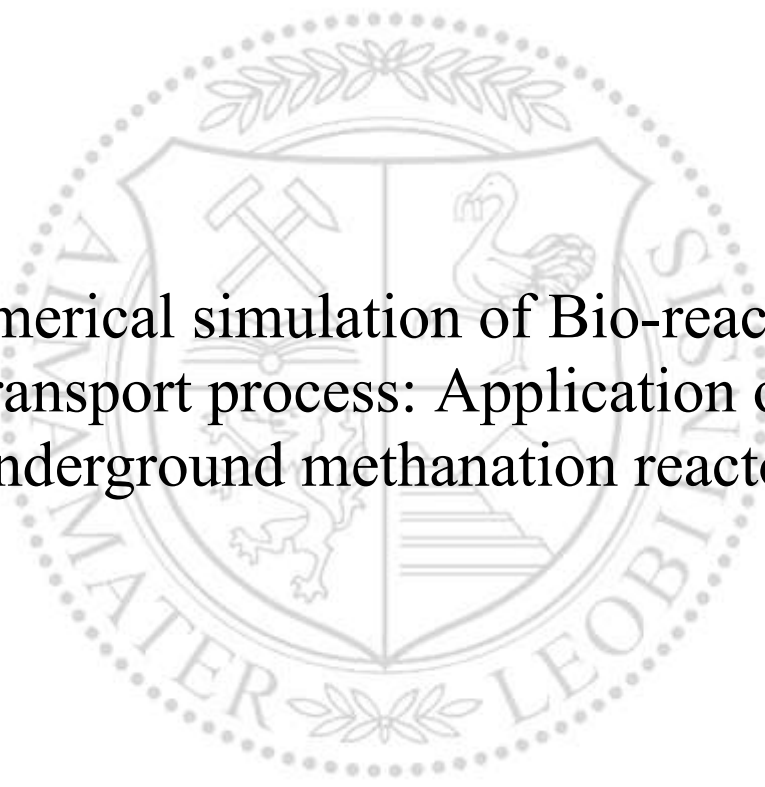Chair of Reservoir Engineering

Master's Thesis

Numerical simulation of Bio-reactive transport process: Application of underground methanation reactor

Denis Nikolaev

November 2020

Dedicated to my beloved family, which supports me throughout my life.

MONTANUNIVERSITÄT LEOBEN
www.unileoben.ac.at

EIDESSTATTLICHE ERKLÄRUNG

I declare on oath that I wrote this thesis independently, did not use other than the specified sources and aids, and did not otherwise use any unauthorized aids.

I declare that I have read, understood, and complied with the guidelines of the senate of the Montanuniversität Leoben for "Good Scientific Practice".

Furthermore, I declare that the electronic and printed version of the submitted thesis are identical, both, formally and with regard to content.

Datum 26.11.2020

Signature Author
Denis Nikolaev

Acknowledgements

Abstract

Power-to-Gas projects is a promising technology for the conversion of renewable energy into green hydrogen and methane. Currently, the renewable sector is investigated in a set of ambitious projects to make advance the energy transition. In principle, Power-to-Gas technology incorporates the conversion of electricity into hydrogen and ultimately into methane via an underground bio-methanation process. This bio-methanation can significantly reduce fossil fuel dependency and carbon footprint. Which is a prominent driver to develop such technology in Germany.

Surplus electricity from variable renewable energy sources has led to employ additional long-term storage capacities such as decommissioned gas storages, depleted oil and gas reservoirs with huge volumes. Another advantage of using these reservoirs is the presence of the required catalyst in a form of microorganism. However, feasibility must be precisely assessed.

As part of the ongoing DBI project ''Bio-UGS'', this thesis aims to establish several numerical simulation models capable of simulating the underground Bio-methanation process in conceptual homogeneous models and a field-scale heterogeneous one. A two-phase multi-component bio-reactive transport model for the simulation of the bio-methanation is implemented in open-source DuMux simulator which is based on C++ code. The results of laboratory experiments cannot be included in this thesis due to time limitation and the gap of knowledge remains. Accordingly, the microbial kinetic parameters are used from the literature sources.

The main focus of the simulation is the methanogenesis reaction. To examine the uncertainty in the conversion rates, a sensitivity analysis is carried out. It allowed to quantitatively evaluate the influence of these uncertainties on the results.

The simulation results in the homogeneous conceptual model initialized with nitrogen indicated that the microbial kinetic parameters have a huge impact. Additionally, the design of the underground bio-methanation is significantly dependent on the well spacing, gas injection-withdrawal rates, and gas composition. The optimal well planning can prevent excessive water from methanogenesis to reach the producer. Finally, the total methane yield is estimated for the power supply of 40 MW.

Zusammenfassung

Power-to-Gas-Projekte ist eine vielversprechende Technologie für die Umwandlung erneuerbarer Energie in grünen Wasserstoff und Methan. Gegenwärtig wird der erneuerbare Sektor in einer Reihe ehrgeiziger Projekte untersucht, um die Energiewende voranzutreiben. Im Prinzip umfasst die Power-to-Gas-Technologie die Umwandlung von Elektrizität in Wasserstoff und schließlich in Methan über einen unterirdischen Biomethanisierungsprozess. Diese Biomethanisierung kann die Abhängigkeit von fossilen Brennstoffen und den Kohlenstoff-Fußabdruck erheblich verringern. Dies ist ein wichtiger Treiber für die Entwicklung dieser Technologie in Deutschland.

Überschüssiger Strom aus variablen erneuerbaren Energiequellen hat dazu geführt, dass zusätzliche langfristige Speicherkapazitäten wie stillgelegte Gasspeicher, erschöpfte Öl- und Gaslagerstätten mit riesigen Volumina eingesetzt werden. Ein weiterer Vorteil der Nutzung dieser Reservoirs ist das Vorhandensein des erforderlichen Katalysators in Form von Mikroorganismen. Die Machbarkeit muss jedoch genau geprüft werden.

Im Rahmen des laufenden DBI-Projekts "Bio-UGS" zielt diese Arbeit darauf ab, mehrere numerische Simulationsmodelle zu erstellen, die in der Lage sind, den unterirdischen Bio-Methanisierungsprozess in konzeptionell homogenen Modellen und einem heterogenen Modell im Feldmaßstab zu simulieren. Ein zweiphasiges, mehrkomponentiges bio-reaktives Transportmodell zur Simulation der Biomethanisierung ist in einem Open-Source-Simulator DuMux implementiert, der auf C++ Code basiert. Die Ergebnisse von Laborexperimenten können aus Zeitgründen nicht in diese Arbeit einbezogen werden, und die Wissenslücke bleibt bestehen. Dementsprechend werden die mikrobiellen kinetischen Parameter aus den Literaturquellen verwendet.

Der Schwerpunkt der Simulation liegt auf der Methanogenesereaktion. Zur Untersuchung der Unsicherheit in den Umstellungsraten wird eine Sensitivitätsanalyse durchgeführt. Sie erlaubt es, den Einfluss dieser Unsicherheiten auf die Ergebnisse quantitativ zu bewerten.

Die Simulationsergebnisse in dem mit Stickstoff initialisiertem homogenem konzeptionellem Modell zeigten, dass die mikrobiellen kinetischen Parameter einen großen Einfluss haben. Darüber hinaus ist das Design der UMR signifikant von den Bohrlochabständen, den Gasinjektions- und -entnahmeraten und der Gasinjektionszusammensetzung abhängig. Eine optimale Bohrlochplanung kann verhindern, dass überschüssiges Wasser aus der Methanogenese zum Produzenten gelangt. Schließlich wird die Gesamtmethanausbeute für die Stromversorgung auf 40 MW geschätzt.

Table of Contents

List of Figures

List of Tables

Abbreviations

DNA   Deoxyribonucleic acid

GIIP   Gas initially in Place

GWC   gas water contact

PEM   Polymer electrolyte membrane

RNA   RNA

SC   Surface conditions

UGS   Underground Gas storage

UHS   Underground Hydrogen storage

UMR   Underground Methanation reactor

<div align="right">

Chapter 1

</div>

Introduction

In recent years, the attention to the renewable sector is growing rapidly due to the intention of the European Union on energy transformation into renewables by 2050 years for 80-95%. This change requires a lot of transformations to the energy sector to provide a constant supply of energy for end-users. One of the challenges associated with renewable energy sources is their fluctuating nature. A possible solution to deal with such fluctuations is to store surplus energy until further demand. Proven economic efficiency is demonstrated by the technology of converting the excess electrical energy through electrolysis into hydrogen and storing it in underground storage facilities. Such operations usually raise many issues related to the integrity of the reservoir, hydrodynamics, well integrity, hydrogen interaction with rock minerals and microorganisms (Strobel et al., 2020). After analysis of the hydrogen interaction with in-situ microbes, the concept of converting the hydrogen into methane utilising microorganisms is developed (Bauer, 2017).

After years of development the concepts of the bio-underground methanation, it is finally at the testing stage. Currently, there is only one project that deals with the underground methanation on the field scale, namely the "Sun Conversion" project conducted by RAG Company. Another project is on the development stage and the field test is planned for execution in 2021, namely the UMAS project where a UGS Berlin will be partially transformed for the conversion purpose.

Even though there is already a pilot test of the underground bio-methanation, it is required to investigate this process more precisely. Thus, by the Federal government of Germany, a Bio-UGS project has purposed where the DBI-Gruppe takes the leading part. Together with other partners, the project aims to cover a variety of aspects including laboratory experiments of the bio-methanation, reservoir simulations, materials investigations and feasibility study.

1.1   Background and Context

A large research project is currently underway at the DBI-Gruppe to investigate the bio-methanation potential and the influencing parameters of this process in porous storage structures. To perform a feasibility study the quantitative results of the process must be obtained.

The main objective of Bio-UGS project is to quantify the potential of converting hydrogen to methane in the potential porous reservoirs of Germany. The total duration of the project is 3 years. The results from project partners will be presented in a final workshop. The work is split into different working packages between the Friedrich Schiller University of Jena, DBI-Gruppe, MicroPro, and Isodetect project partners.

The Friedrich Schiller University (FSU) of Jena is a leading partner for the reservoir characterization and selection of representative core sample materials. Within this work package, the lithological and chemical evaluation of core samples provided by underground gas storage operators will be performed. At the same time, additional geological and mechanical properties of reservoir rocks will be obtained from publicly available data. Based on all this information, reservoir models will be constructed. That will serve as a database for the project.

On the next step, investigations of fluid-rock interactions in reservoir rocks and their effects on biological processes will be measured in laboratories of FSU. This will include measuring petrophysical properties, laboratory tests on corrosive behaviour, gas analyses to differentiate between biotic and abiotic reactions, as well as tests on reservoir water samples. This also includes an analysis of reactions with regards to minerals stability. Possibilities of existing software that capable to implement the microbial processes will be analysed by DBI. MicroPro is a leading partner for work packages related to the characterization of the hydrogen-related stimulation of microbial processes in pore structure as well as long-term model tests for microbiological process optimization and risk assessment. All the investigations from this work package will be done in cooperation with Isodetect.

Having measured all laboratory analyses, DBI will start modelling the microbiological processes on a field scale. During this work package reaction kinetics of the microorganisms and gas conversion processes from laboratory tests will be implemented in reservoir simulation software.

1.2   Scope and Objectives

The Bio-UGS project, as the focus of my master's thesis, is aimed at identifying the potential of German fields for an underground methanation reactor (UMR).

This work includes a theoretical and practical study of the processes related to the underground methanation reactor. The theoretical study relates to the hydrodynamic behaviour during the hydrogen and carbon dioxide co-injection as well as the review on microbial processes.

The practical part is divided into two parts. In the first part, the design parameters of the underground bio-methanation are discussed. For that purpose, some simulation results of the homogeneous conceptual model are presented. In the second part, the heterogeneous field-scale model is built based on the general reservoir characteristic of the German reservoir formations. The purpose of creating such a reservoir model is to honour the heterogeneity that may influence the operation. This model includes heterogeneity in porosity and permeability distributions, the simple structure and depth of one real reservoir. Those complexities are applied for honouring the depositional environments as control of reservoir features and subsequently the hydrodynamic processes.

The underground methanation process is new and not fully developed concept. The mathematical model and developed code for population dynamics and bio-reactive transport flow are used from previous studies. The model includes methanogenic and sulfate-reduction bio-reactions. The research is done by Hagemann as a part of H_2STORE project who developed the DuMux code for such a process to simulate underground hydrogen storage (Hagemann, 2018). The application of the developed code is extended to the methanation process on a homogeneous 2D case. The 3D case is presented in this thesis by employing more complex reservoir model. The development strategy mimics the co-injection of carbon dioxide and hydrogen from an electrolyser powered by 40 MW from a wind park.

1.3   Overview of Thesis

In the second chapter, the important aspects related to the underground hydrogen and bio-methanation process are discussed. In general, this process can be subdivided into two major steps: co-injection of hydrogen and carbon dioxide into the reservoir and further conversion of the injected gases into methane via microbial metabolism.

In the first and second sections of the third chapter, the fundamentals of two-phase flow and multicomponent transport are explained. In the last section, a mathematical model used in the multi-physics simulator DuMux is discussed which is an open-source framework that allows the simulation of multiphase fluid flow and transport processes in porous media. It provides a

set of different model concepts, constitutive relations, as well as the discretization schemes and solvers (Flemisch et al., 2011).

The last chapter deals with simulation. It is divided into two sections. In the first section, there the results of the simulation of the homogeneous grid are presented. An influence of different operational parameters is explained for the case of a reservoir filled with nitrogen. The effect of the well spacing on methane pureness is discussed in this subchapter. In the second section, there are results from the simulation of heterogeneous field scale grid. The simulation imitates the storage scenario in the reservoir filled with methane. The main focus of the thesis is the produced methane out of methanogenic archaea.

<div align="right">

Chapter 2

</div>

Literature review

In this chapter, the important aspects related to the underground hydrogen and bio-methanation process are discussed. In general, this process can be subdivided into two major steps: co-injection of hydrogen and carbon dioxide into the reservoir and further conversion of the injected gases into methane via microbial metabolism.

Thus, it is required to explain the hydrodynamic behaviour in such a complex system and the relevant microbial processes associated with methanation. The processes related to the integrity of the reservoir and cap rock are not part of this thesis.

2.1   Hydrodynamic behaviour during hydrogen storage

There are different types of underground gas storage mechanism. Gas can be stored in the porous structure of natural aquifers, depleted oil/gas fields and salt caverns. In this subchapter, the hydrodynamic behaviour associated with hydrogen storage in aquifers and depleted gas fields will be discussed.

2.1.1 Storage in aquifer

During hydrogen storage in aquifer, one could expect a quite significant mobility ratio between displacing and displaced fluid around 100 and strong differences in density. It would lead to unstable displacement which manifests in gravity override and fingering (Feldmann et al., 2016). It worth to mention some other phenomena that occur together with fingering. Usually, the displacing front becomes heterogeneous and tip splitting occurs. It is a phenomenon when the tip of a finger splits into two branches. The second phenomenon causes the lateral spreading that unites the fingers and making the displacement more stable. Another phenomenon called shielding causes the growth of one finger that growing much faster than others (Ho & Webb, 2006). Tip splitting and shielding can be seen in Figure 2-1. Gravity override phenomenon with real storage sites examples is discussed in (Tek, 1989).

Figure 2-1. Tip splitting (top) and shielding (bottom) in viscous fingers (Ho & Webb, 2006)

The highly mobile hydrogen injection into the aquifer could also lead to an uncontrolled spreading of hydrogen along with the cap rock structure. That finally will cause leakage of the gas beyond the cap rock (Figure 2-2).
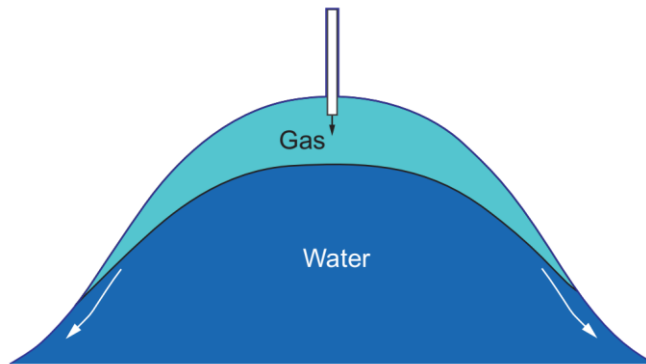
Figure 2-2. Lateral spreading of hydrogen (Panfilov, 2016)

However, such leakage can be avoided in several cases. In aquifers of steep structures, the lateral migration can be prevented (Sainz-Garcia et al., 2017). Another controlling parameter can be the injection rate. When the injection rate is low, the gravity and capillary forces can dominate over viscous forces (Tek, 1989). Thus, the displacement can be more stable. This statement is confirmed in (Hagemann et al., 2016) with numerical reservoir simulations. Where

a couple of scenarios of hydrogen injection into a depleted gas reservoir with different injection rates are simulated.
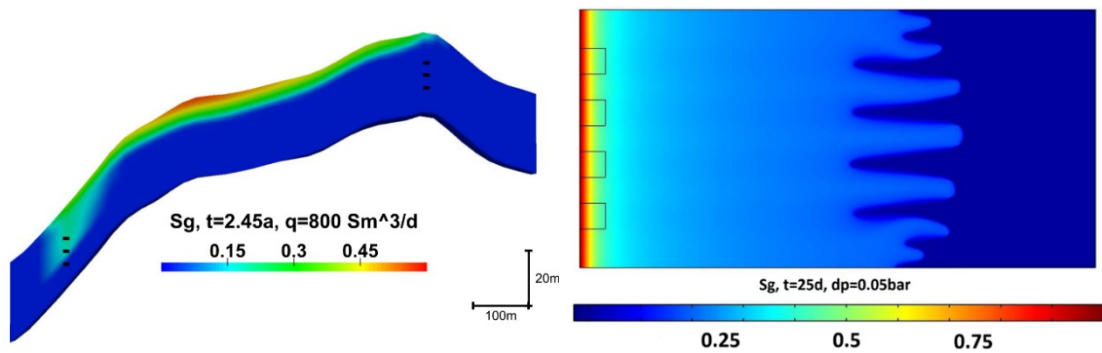
Figure 2-3. Water displacement by hydrogen. Left - vertical cross-section; Right - horizontal cross-section (Feldmann et al. 2016)

In (Feldmann et al., 2016) comparison between hydrogen storage in the aquifer and the depleted gas reservoir is done numerically. The hydrogen injection revealed strong gravity override which is explained by the high difference in densities of hydrogen and water. It is also shown that with a small heterogeneity in permeability, the displacing front becomes completely unstable and viscous fingers start to develop (Figure 2-3).

2.1.2 Storage in gas reservoirs

In contrast to aquifers, the hydrogen storage in depleted gas reservoirs can reveal less viscous instabilities due to the lower mobility ratio between hydrogen and natural gas. The typical properties for hydrogen, methane can be seen in Table 2-1.

Table 2-1. Physicochemical properties of hydrogen, methane(Alcock J. L. et al., 2001) and (Das, 2016)

Properties	Hydrogen	Methane
Molar mass [g/mole]	2.016	16.043
Density at SC [kg/m^3]	0.08375	0.6682
Heating value [kJ/g]	120–142	50–55.5
Flammability limits [vol% in the air]	4–75	5.3–15
Minimum ignition energy [mJ]	0.02	0.29
Auto ignition temperature [°C]	585	540
Detonability limits [vol% in the air]	11–59	6.3–13.5
Diffusion coefficient in air at SC[cm^2/s]	0.61	0.16

In reservoir conditions, one can expect a mobility ratio between hydrogen and methane around 1.5 which is two orders of magnitude lower to the one in hydrogen and water system. Hence, such unfavourable phenomena as lateral leakage, fingering and gravity override should have a minor effect.

In (Feldmann et al., 2016) the numerical simulation study showed relatively uniform displacement of the reservoir gas by hydrogen. No major lateral spreading of hydrogen is seen (Figure 2-4). In (Hagemann, 2018) it is shown that the injection rate plays a dominant role in controlling the displacement front and homogeneous hydrogen injection.

For the sake of the stable injection of hydrogen, several cases show the best permanence. They include the injection of hydrogen in depleted gas reservoirs or reservoirs with alternative gas. In several studies, it is concluded that alternative cushion gas shows better performance comparing to aquifer storage. Thus in (Pfeiffer et al., 2015), nitrogen is suggested as alternative cushion gas. In (Oldenburg, 2003) a carbon dioxide is suggested as a cushion gas for gas storage.

In Feldmann et al., 2016 and Hogeweg et al., 2020, nitrogen is used as cushion gas for simulation the underground hydrogen storage. Concerning the hydrodynamic behaviour, no issues are observed.
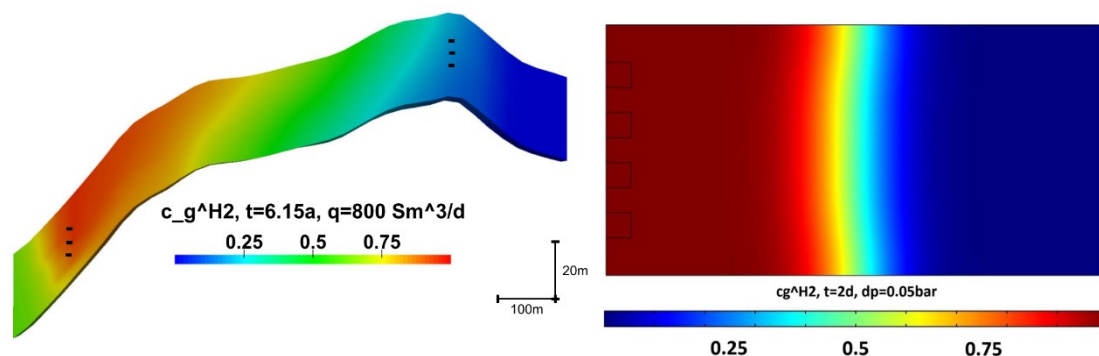
Figure 2-4. Gas displacement by hydrogen. Left - vertical cross-section; Right - horizontal cross-section

2.1.3 Effect of Microorganisms on Hydrogen distribution

In (Hagemann et al., 2016) an effect of methanogenesis bacteria on hydrodynamic behaviour is analysed. It is concluded that methanogenesis bacteria limits the diffusion of nutrients. That's is why hydrogen and carbon dioxide distribution is expected to be less spread.

2.2 Microbial processes

In this thesis, the terms "microorganisms", "bacteria" And "Archaea" are used as identical.

2.2.1 Microbial morphology

Microbes are defined as microscopic organisms that cannot be seen by the human naked eye. Based on similarities in ribosomal RNA, the microbes can be classified as Archaea and Bacteria. The typical size of the microbial cell is 0.2–1.5 μm in diameter and 3-5 μm in length (Ananthanarayan & Paniker, 2008). Most Bacteria appear in variations of three shapes which are rod, sphere, and spiral shapes. However, other odd shapes can be observed as well. Bacteria can be arranged in single, pairs, groups, clusters, or even cubes. The idealized bacteria structure is formed by a rigid cell wall with a cytoplasmic or plasma membrane beneath it. The cell envelope consists of protoplasm, cytoplasmic inclusions, and nuclear body (Ananthanarayan & Paniker, 2008).

2.2.2 Microbial growth

Microbial growth is represented by increasing cell concentration. The increased cell concentration is associated with an increased number of cells or cell mass. The most common quantitative characteristic of bacterial growth is cell concentration over time (Mohanta et al., 2017). The typical mechanism which is responsible for bacteria cell replication is binary fission. The binary fission defines cell replication by cell division (Parker et al., 2018). After a bacterial cell has reached a certain size, it starts to divide into two daughter cells (Figure 2-5). The time required for the cell division is called generation time or population doubling time. Theoretically, the bacterial growth in a relatively short period of time can reach enormous concentration and mass. In practice, however, the bacterial growth is limited by depletion of nutrients or accumulation of toxic elements (Ananthanarayan & Paniker, 2008). For subsurface conditions, another limiting factor is heterogeneity that results in cells being separated from each other. Accordingly, they cannot share nutrients or protection mechanisms together (Maier et al., 2009).
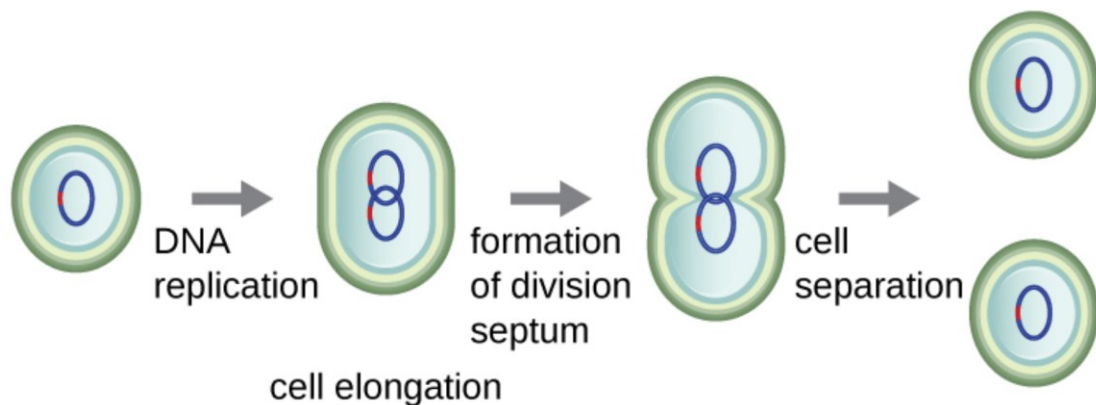
Figure 2-5. Cell duplication by binary fission (Ananthanarayan & Paniker, 2008)

Microbial growth requires energy that comes from metabolism. According to (Maier et al., 2009) there are four types of metabolism, namely, chemoheterotroph, chemoautotroph, photoautotroph, and photoheterotroph. They are different from each other in terms of energy and carbon sources. The source of energy can be obtained either from light or from the oxidation of chemicals. Whereas carbon source is carbon dioxide or organic compounds.

Growth of bacterial can be studied by batch culture or continuous culture experiments. Batch culture experiment represents a closed system culture where bacterial are growing at specific environmental conditions. The conditions can be defined by the specific nutrient type and its fixed amount, temperature, pressure, etc. A general bacterial count versus time for a batch experiment is shown in (Figure 2-6). Usually, the bacterial population is characterized by 4 steps.

Lag phase: Follows after the start of the experiment when there is no increase in the number of bacterial. During this phase, the nutrients are already present in the system and other conditions are favourable for growth. The lag phase is defined from the beginning of the experiment till the exponential phase begins. During this phase, microbes are inactive in terms of the population number. The constant number of the population is also explained by the physiological adaptation of the cells to newly introduced conditions (Parker et al., 2018). Notably, the number of cells does not increase during this phase. However, microorganisms still consume nutrients. This is due to the fact, that microbial consume nutrients for growing in size of an individual cell (Panfilov, 2018). This is also reflected in increasing the mass gain of each bacteria.

Log (Exponential growths) phase follows the lag phase. During the log phase, the bacterial cells start duplication, and thus, the number of cells growing exponentially or by geometric progression. In the case of geometric progression, the number of cells after n divisions will be 2^n (Parker et al., 2018).
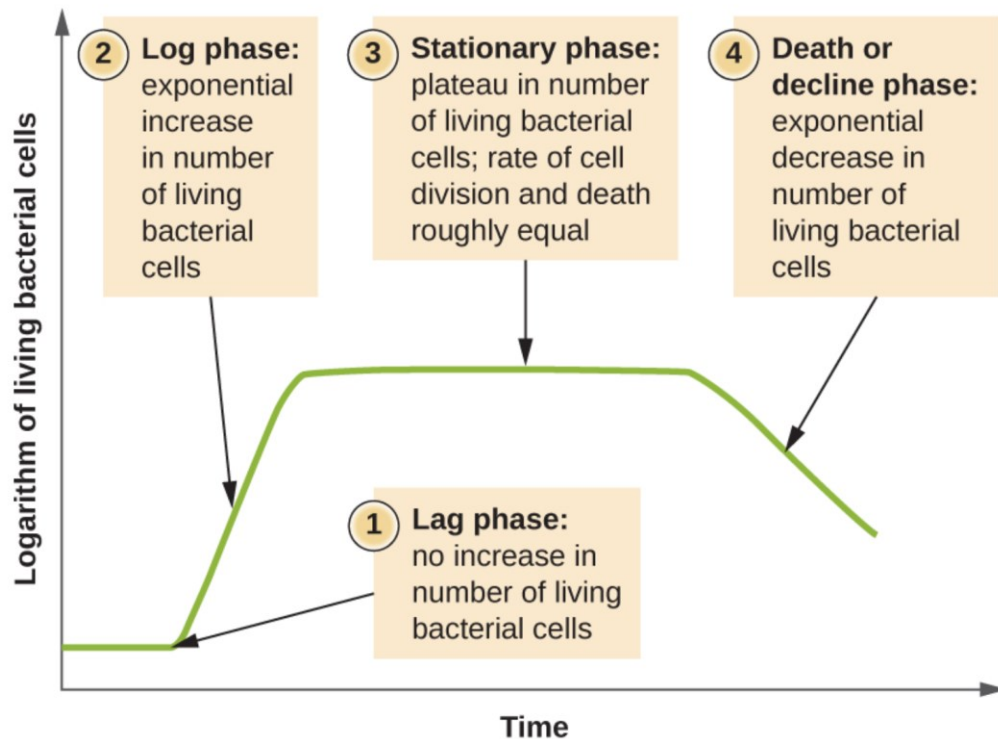
Figure 2-6. The growth curve of bacterial (Parker et al., 2018)

Stationary phase: Follows the lag phase when the number of microorganisms stays constant. This is related to a lack of nutrients and a certain accumulated portion of toxic products. The number of progeny cells becomes sufficient just to balance the dying cells (Ananthanarayan & Paniker, 2008).

Decline (death) phase: The last phase follows the stationary phase. During this phase, the number of cells decreases due to microbial cell death. The cells reduction caused by total nutrients exhaustion and accumulation of toxic elements. The phase is also characterized by exponential behaviour, however, the decay rate is usually lower than the growth rate. (Maier et al., 2009).

2.2.3 Form of existence

Three main forms of existence of microorganisms are considered in the literature (Panfilov, 2018):

- Biofilm: It is a group of microorganisms that are living together mostly on solid surfaces in the water.
- Plankton: It is a collective of microorganisms that live in a large volume of water without being able to swim against the current (Lalli & Parsons, 1997).
- Neuston: They are organisms that living in the water on gas and water interface (Merriam-Webster, 2020).

2.2.4 Microbial movement

The bacterial transport is different for every form of existence. In terms of transport, plankton can be characterized as the most active ones. To describe its movement one distinguishes the advection-diffusion way of transport (Panfilov, 2018). Whereas the movement of biofilm is more complex. The biofilm is usually formed in stagnant zones of pore structures that are associated with low fluid flow speed (Hassannayebi, 2019). However, once the flow velocity increases, the bacteria can be detached from the biofilm and transported by the flow. That is why such a process should be formulated as advection transport with trapping (Panfilov, 2018).

2.2.5 Metabolism of microorganisms

Metabolism of bacteria can be divided into two different types: respiratory metabolism and constructive metabolism (nutrition).

During respiration, there is no change in biomass. The bacterial can consume hydrogen and carbon dioxide only for respiration. The respiration causes also the transformation of reactants into other chemical substances (Panfilov, 2016). In the case of the methanogenic reaction, the products of the reaction are methane and water.

Nutrition is followed by the production of biomass. It differs in the way that external organic or inorganic carbon is transformed into organic substances. Later, these substances are used for the biomass generation (Panfilov, 2016). However, the chemical products of nutrition are the same as those for respiration.

2.2.6 Microbial reactions

In many aspects, underground methanation is similar to underground hydrogen storage (Strobel et al., 2020). The most relevant reactions for underground hydrogen storage (Hagemann, 2018) catalysed by hydrogenotrophic bacteria are:

- Methanogenesis:

$$CO_2 + 4H_2 \longrightarrow CH_4 + 2H_2O \tag{2.1}$$

- Acetogenesis:

$$2CO_2 + 4H_2 \longrightarrow CH_3COOH + 2H_2O \tag{2.2}$$

- Sulphate-reduction:

$$SO_4^{2-} + 5H_2 \longrightarrow H_2S + 4H_2O \tag{2.3}$$

- Iron(III)-reduction:

$$3Fe_2^{III}O_3 + H_2 \longrightarrow 2Fe_3^{II}O_4 + H_2O \tag{2.4}$$

<div align="right">
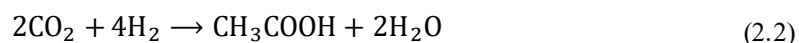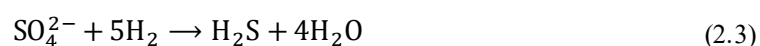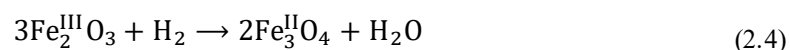
Chapter 3

</div>

Fluid flow fundamentals and mathematical model

In the first and second sections of this chapter, the fundamentals of two-phase flow and multicomponent transport will be explained.

In the last section, a mathematical model used in the multi-physics simulator DuMux will be discussed. DuMux is an open-source framework that allows the simulation of multiphase fluid flow and transport processes in porous media. It provides a set of different model concepts, constitutive relations, as well as the discretization schemes and solvers (Flemisch et al., 2011).

3.1   Two-phase flow

Multiphase flow characterizes the system where at least two separate phases are present. Then each phase has its own physical and chemical properties. In such a case one can introduce wetting and non-wetting phases. Thus, there is an interfacial tension between the phases that causes capillary pressure in porous structures.

Advection is a fluid flow caused by pressure gradients. In Figure 3-1 the advection during two-phase is shown. The velocity vector of the displacement is controlled by the pressure gradient. Thus, fluid A is displacing fluid B in the right direction because p_1 is higher than p_2. Generally, advection can be characterized by Darcy's law.   Advection is a transport mechanism of components that is stronger and faster than diffusion.
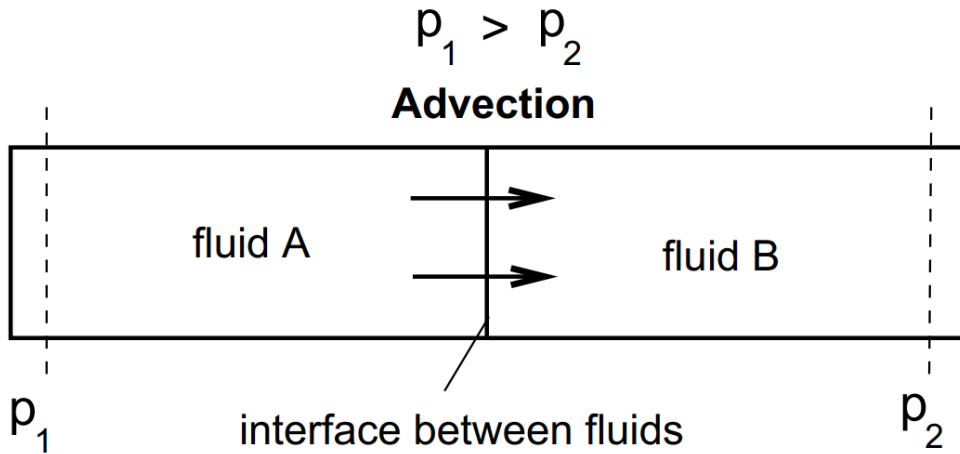
Figure 3-1. Advection in multi-phase flow (Bielinski, 2007)

3.1.1 Capillary pressure

Capillary pressure (P_c) is also defined as a pressure difference between the pressure of the non-wetting phase (P_g) and wetting phase (P_w):

$$P_c(S_w) = P_g - P_w$$

(3.1)

In a two-phase system, the entry capillary pressure must be exceeded by the non-wetting phase to enter the pore space. For sandstone rocks with good reservoir quality, the entry capillary pressure is orders of magnitudes smaller than for typical shale reservoir cap rocks for the same fluid system. Usually, capillary trapping in shale cap rock is the main mechanism for sealing the reservoir gas. Thus, as long as the capillary entry pressure is not exceeded the gas could not flow through the cap rock. (Reitenbach et al., 2015)

3.1.2 Relative permeability

In the multiphase system, Darcy's law can be extended by introducing relative permeability. The relative permeability is a function of the fluid saturation and the wetting characteristics of the porous media. It controls the fluid flow of the separated phases.

In this model, capillary pressure and relative permeability for the two-phase system are calculated using Brooks and Corey formulation (Corey, 1964).

3.2   Compositional Multicomponent transport

3.2.1   Mole fractions

Every phase in the model consists of several components. The quantity of the component is defined by mole fraction, which is the number of the moles n of the κ component in the α phase in the total number of moles in the same phase:

$$c_\alpha^\kappa = \frac{n_\alpha^\kappa}{\sum_i n_\alpha^i}$$

(3.2)

Mole fractions of all components for each phase are equal to 1.

$$\sum_k c_w^k = 1 \quad \sum_k c_g^k = 1$$

(3.3)

3.2.2   Hydrodynamic dispersion

Hydrodynamic dispersion refers to both molecular diffusion and mechanical dispersion.

Diffusion is a transport mechanism caused by the thermal motion of molecules (Meyers, 2002). It explains the flux of a certain component from a region with a high concentration into the region with a lower concentration. Unlike dispersion or advection, the diffusion flux is independent of orientation and velocity. Typically diffusion is characterized by Fick's law (Fick, 1855). For the dissolved component the mass flux is considered as follows:

$$J_w^k = -\rho_w D_{\text{diff},w}^k \nabla c_w^k$$

(3.4)

where $D_{\text{diff},w}^k$ is the effective molecular diffusion coefficient of component k in water in (m^2/s), ∇c_w^k is the composition gradient.

Mechanical dispersion consists of micro-and macro-dispersion. Micro-dispersion is a pore-scale parameter caused by the parabolic velocity profile in the pore space between mineral grains. While macro-dispersion is caused by velocity variation in the rock. The velocity varies due to the macroscopic heterogeneity of the rock. Both dispersions are defined as a function of the fluid velocity. The maximum value of the dispersion corresponds to the direction of the velocity vector, while the minimum is perpendicular to it (Tek, 1989).

3.2.3   Phase equilibrium calculation

There is a common practice for phase composition calculation when equilibrium ratios are formulated as:

$$K_k = \frac{c_g^k}{c_l^k}, \; k = 1, \ldots, n \tag{3.5}$$

Which leads to the determination of the total balance of the gas and liquid compositions relationship (Panfilov, 2018):

$$C_k = c_g^k \sigma + c_l^k (1 - \sigma), k = 1, \ldots, n \tag{3.6}$$

where σ is the mole fraction of the gas phase, C_k is the total mole fraction of component k in the mixture.

The relations (3.5) and (3.6) can be rearranged for:

$$\sum_{k=1}^{n} \frac{C_k}{\sigma + K_k(1 - \sigma)} = 1 \tag{3.7}$$

Then the compositions can be calculated by the following steps:

- Equation (3.29) has to be solved for σ
- The component concentration in the gas phase c_g^k is calculated via the equation:

$$c_g^k = \frac{C_k}{\sigma + K_k(1 - \sigma)}$$

- Finally, the component concentration in the liquid phase c_l^k is obtained from:

$$c_l^k = c_g^k / K_k.$$

The equilibrium ratios can be calculated using Raoult's, Dalton's for ideal solutions. According to Raoult's, the partial pressure p^k of a component in a multicomponent system is equal to multiplication of the component mole fraction c_w^k and its vapour pressure p_g^k (Ahmed, 2010).

$$p^k = c_w^k p_g^k \tag{3.8}$$

Whereas, Dalton's law states that partial pressure of a component in a multicomponent system is equal to multiplication of the component mole fraction in vapour c_g^k and the total pressure of the system P (Ahmed, 2010).

$$p^k = c_g^k P \tag{3.9}$$

Henry's law is considered:

$$c_w^k = H_k c_g^k P \tag{3.10}$$

where H_k is the Henry solubility [Pa⁻¹]. The equation is applicable only for solutes in low concentrations in liquid (Panfilov, 2018).

Thus, the equilibrium ration can be formulated:

$$K_k = \frac{c_g^k}{c_w^k} = \frac{p_g^k}{P} = \frac{1}{H_k P} \qquad (3.11)$$

3.3 The mathematical model in DuMux code

To be able to simulate Underground Methanation Reactor (UMR), the simulation model must take into account not only microbial population dynamics but also the compositional hydrodynamic model that considers hydrogen, carbon dioxide, and methane. Such a coupled mathematical model is developed by (Hagemann et al., 2014). Initially, it is implemented to simulate Underground Hydrogen Storage (UHS). Later by (Hogeweg et al., 2020), the developed code is successfully examined for the purpose of UMR simulation. The model is on a macroscopic scale, it considers two phases (gas and water). In this sub-chapter, some essential parts of the mathematical model developed by (Hagemann et al., 2014) will be described.

3.3.1 Physico-chemical processes

The transport of components within the flowing phases is formulated by a flux term with a certain component in the phases. The chemical component mass conservation, advective, and dispersive/diffusive transport is formulated as:

$$\phi \frac{\partial\left(\rho_g c_g^k S_g + \rho_w c_w^k S_w\right)}{\partial t} + \nabla \cdot \left(\rho_w c_w^k v_w + J_w^k + \rho_g c_g^k v_g + J_g^k\right) = q^k \qquad (3.12)$$

where ϕ is the porosity; ρ is the molar density in (mol/m^3); c is the mole fraction of the k component in the w – water, or g – gas phase; S is the saturation; v is the advective flux in (m/s); J is the dispersive/diffusive flux in (mol/m^2/s); q is used to model the source/sink of the specific component inside the model domain or at boundaries.

Momentum conservation is considered by Darcy's law:

$$v_i = -\frac{K k_{ri}}{\mu_i} \cdot (\nabla P_i - \hat{\rho}_i g), i = g, w \qquad (3.13)$$

where K describes the absolute permeability in (m^2), k_r is the relative permeability, μ is the dynamic viscosity in (Pa·s), P is the phase pressure in (Pa), $\hat{\rho}$ is the phase density in (kg/m^3), and g is the gravitational acceleration in (m/s^2).

The dispersion/diffusion term is formulated individually for the gas and the water phase. Fick's law (Fick, 1855) is considered to determine the diffusive-dispersive flux in the water phase:

$$J_w^k = -\rho_w \left(D_{\text{diff},w}^k + D_{\text{disp},w}^k \right) \nabla c_w^k \qquad (3.14)$$

where $D_{\text{diff},w}^k$ is representative of the effective molecular diffusion coefficient of component k in water in (m²/s) and $D_{\text{disp},w}^k$ is the mechanical dispersion coefficient of component k in water in (m²/s). Within the gas phase, the diffusion-dispersion term can be defined by Blanc's law (Poling et al., 2000):

$$J_g^k = -\left(\sum_{j=1 \neq i}^{n} \frac{c_g^j}{\rho_g D_{\text{diff},g}^{ij}} \right)^{-1} \nabla c_g^k - \rho_g D_{\text{disp},g}^k \nabla c_g^k \qquad (3.15)$$

where $D_{\text{diff},g}^{ij}$ is the effective binary diffusion coefficient between component i and component j in (m²/s).

Capillary pressure and relative permeability are used to honour two-phase flow. One of the ways for formulating them is the Brooks-Corey correlation (Corey, 1964):

$$S_{\text{we}} = \frac{S_w - S_{\text{rw}}}{1 - S_{\text{rw}} - S_{\text{rg}}} \qquad (3.16)$$

$$P_c(S_w) = P_e S_{we}^{-\frac{1}{\lambda}} \qquad (3.17)$$

$$k_{rw}(S_w) = S_{we}^{\frac{2+3\lambda}{\lambda}} \qquad (3.18)$$

$$k_{rg}(S_w) = (1 - S_{we})^2 \left(1 - S_{we}^{\frac{2+\lambda}{\lambda}} \right) \qquad (3.19)$$

where S_{we} is the effective water saturation, S_{rw} and S_{rg} are the residual saturations for wetting and non-wetting phases, respectively, and the subscript P_e denotes the entry capillary pressure in (Pa) and λ refers to the pore size distribution index. At the same time, the difference between wetting and non-wetting phase's pressures are controlled by capillary pressure:

$$P_c(S_w) = P_g - P_w \qquad (3.20)$$

3.3.1.1 Density and viscosity

By assuming ideal gas law behaviour the gas phase density can be calculated as follows:

$$\hat{\rho}_g = \frac{P_g \sum_{k=1}^{7} c_g^k M^k}{RT} \qquad (3.21)$$

where M is the molar mass in [kg/mol], R is the gas constant in [J/mol/K] and T is the temperature in [K]. Water phase density is calculated based on its composition.

The viscosity of the gas phase is calculated using the Wilke method (Poling et al., 2000) and water phase viscosity is constant and equal to 1 cP.

3.3.1.2 Phase equilibrium calculation

In total, the model takes into account seven components. DuMux provides an extensive library for components properties. However, for some components, the properties are not present. That's why in the work of (Hagemann et al., 2014) the relevant properties for hydrogen are added into the DuMux library employing known correlations.

Phases compositions for a given temperature, pressure are calculated under the assumption of thermodynamic equilibrium (Hagemann et al., 2016). This assumption suggests that fugacities of a component in both phases are equal:

$$f_g^k = f_w^k \quad \text{or} \quad c_g^k \varphi_g^k P_g = c_w^k \varphi_w^k P_w \tag{3.22}$$

where f is the parameter of the fugacity in [Pa] and φ is the fugacity coefficient. Considering ideal gas behaviour, the fugacity coefficients of the gaseous component in the gas phase are equal to 1.

Fugacity coefficients of gaseous components in the water phase are calculated using Henry's law:

$$\varphi_w^k = \frac{H_k}{P_w} \tag{3.23}$$

where H is Henry's law constant in [Pa]. The fugacity coefficient of the water component by itself is calculated via vapour pressure:

$$\varphi_w^{H_2O} = \frac{P_v^{H_2O}}{P_w} \tag{3.24}$$

where $P_v^{H_2O}$ is the vapour pressure of pure water in [Pa]. Mole fractions of all components for each phase are equal to 1.

$$\sum_k c_w^k = 1 \quad \sum_k c_g^k = 1 \tag{3.25}$$

3.3.1.3 Bio-chemical processes

In order to model, microbial processes on the Darcy scale, some simplifications have to be used. The reservoir model is initialized only with residual water saturation. That is why the advective transport in the water phase can be neglected and thus, advective transport of microorganisms

too. The chemotaxis (microbial orientation towards nutrients) of microbes is neglected due to different scales in microbial processes and fluid flow formulation. Microbial population dynamics be described as follows (Hagemann et al., 2014):

$$\frac{\partial n}{\partial t} = S_w \psi^{\text{growth}} \left(c_w^S, c_w^A \right) \cdot n - \psi^{\text{decay}} \cdot n + \nabla \cdot (D_m \nabla n)$$

(3.26)

where n represents the number of microorganisms in $(1/m^3)$, ψ^{growth} is the microbial growth function in $(1/s)$, which is the function that depends on the substrate concentration c_w^S and the electron acceptor concentration c_w^A in the water phase, ψ^{decay} is the decay in $(1/s)$, and the last term D_m is the microbial diffusion coefficient in (m^2/s). The decay here is considered by a constant value. Since the degradation of the substrate is followed by microbial growth, the bio-chemical reactions can be considered:

$$q^k = \phi S_w \gamma^k \frac{\psi^{\text{growth}}}{Y} n$$

(3.27)

where γ is the stoichiometric coefficient related to the reaction equations and term Y denotes the yield coefficient, which is the ratio between the reproduction of microorganisms and the consumption of substrates.

The double Monod equation, which is extended by (Megee et al., 1972) is used for describing the microbial growth function. It is formulated by:

$$\psi_m^{\text{growth}} = \psi_{m,max}^{\text{growth}} \left(\frac{c_w^S}{\alpha_{m,1} + c_w^S} \right) \left(\frac{c_w^A}{\alpha_{m,2} + c_w^A} \right)$$

(3.28)

where $\psi_{m,max}^{\text{growth}}$ refers to the maximum specific growth rate in $[1/s]$, α is the half-velocity constant, and m microbial species (methanogenic archaea, sulphate-reducing bacteria). Several experiments are conducted to obtain the microbial kinetic parameters. The summed up version of these parameters can found be in (Hagemann, 2018).

3.3.2 A coupled system of equations

In the precise mathematical model that can describe both the microbial population and multi-component two-phase flow, all mentioned equations in the bio-chemical and Physico-chemical processes must be coupled.

The original mathematical model considers four reactions. However, only methanogenic archaea are considered in the numerical simulation part of the thesis.

The governing system of equations consists of microbial population dynamic and reactive transport for mobile components (Hagemann et al., 2014).

The microbial population dynamics is defined as follows:

$$\frac{\partial n_m}{\partial t} = S_w \psi_m^{\text{growth}} \cdot n_m - \psi_m^{\text{decay}} \cdot n_m + \nabla \cdot (D_m \nabla n_m), m = M, S \tag{3.29}$$

Coupled bio-reactive transport is considered by the following equation:

$$
\begin{aligned}
&\phi \frac{\partial(\rho_g c_g^k S_g + \rho_w c_w^k S_w)}{\partial t} \\
&+\nabla \cdot \left(-\rho_g c_g^k \frac{K k_{rg}}{\mu_g} \cdot (\nabla P_g - \hat{\rho}_g g) - \rho_w c_w^k \frac{K k_{rw}}{\mu_w} \cdot (\nabla P_w - \hat{\rho}_w g) \right) \\
&+\nabla \cdot \left(-\rho_g (D_{\text{diff},g}^k + D_{\text{disp},g}^k) \nabla c_g^k - \rho_w (D_{\text{diff},w}^k + D_{\text{disp},w}^k) \nabla c_w^k \right) \\
&= \phi \sum_m \gamma_m^k \frac{\psi_m^{\text{growth}}}{Y_{m,e}} n_m \\
&\qquad k = H_2, CO_2, CH_4, N_2, C_2H_6, C_3H_6, H_2O, SO_4^{2-}
\end{aligned}
\tag{3.30}
$$

3.3.3 Boundary conditions

There are two types of boundary conditions are used in the developed code. The first type is the Dirichlet boundary condition that fixes the absolute value of the primary variable which can be time depended. The second type is the Neumann boundary condition which is used for the time-dependent definition of molar fluxes for respective boundaries. These fluxes are linked to the source/sink term in the mass conservation equation.

<div align="right">

Chapter 4

</div>

Simulation

This chapter is divided into two sections. In the first section, there are results from the simulation of the homogeneous grid. An influence of different operational parameters is explained for the case of a reservoir filled with nitrogen. The effect of the well spacing on methane pureness is discussed. In the second section, the simulation results of the heterogeneous field scale are presented. The simulation imitates the storage scenario in the reservoir filled with methane. The main focus of the thesis is the produced methane out of methanogenic archaea.

4.1   Operational parameters

Here is the subchapter of results from a simple grid. Where the importance of distances between the wells, injection rate and composition are explained.

4.1.1 Model domain and properties

The model in this subchapter has the parameters specified in Table 4-1.

Table 4-1. Initial parameters of the homogeneous model

Parameter	Value	Unit
GWC	1050	m
Pressure @ GWC	90	bar
Temperature	40	^{o}C
Kxx, Kyy, Kzz	200	mD
Porosity	20	%
GIIP	6.03E+06	rm^3
Number of grid cells	2350	-
Grids dimensions	50x50x3	m
Initial composition:		
N$_2$	100	%

The reservoir thickness is 15m. The grid cell size is 50x50x3m with the total number of grid cells around 3000 (Figure 4-1).
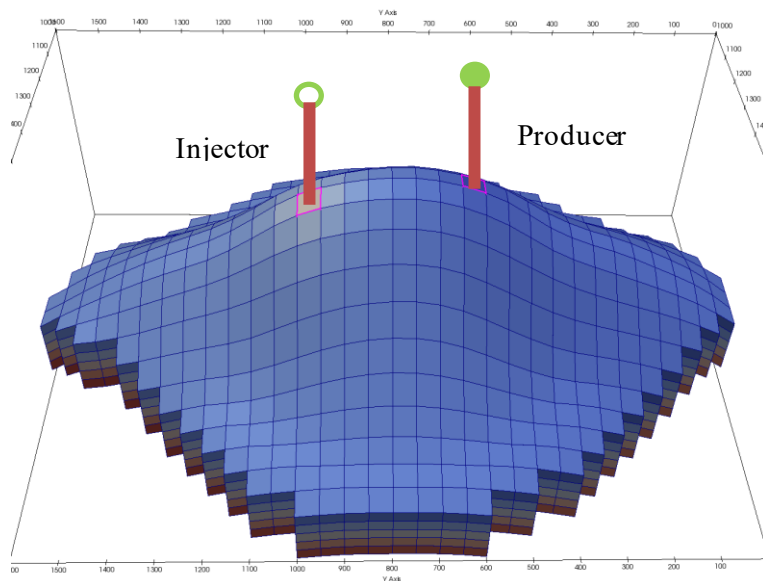
Figure 4-1. Model grid with dimensions and wells positions

The methods used for the calculation of fluid properties are described in section 3.3.

The relative permeability and capillary pressure are calculated based on the Brooks-Corey equation (Figure 4-2). The procedure is explained in the mathematical model section. The parameters used for the model are as follows:

- Residual water saturation S_{rw}: 0.1
- Residual gas saturation S_{rg}: 0.1
- Capillary entry pressure Pe: 100000 Pa
- Lambda λ: 2

Figure 4-2. Relative permeability (left) and capillary pressure (right) used for the model

4.1.2 Numerical simulation

The first step of the simulation is the initialisation step. The reservoir is initialized assuming the hydrostatic equilibrium. Thus, the pressure of the gas zone, transition, and water zone is calculated based on pressure gradients and capillary pressure. The pressure is defined at the gas-water contact at a certain depth. All boundaries are defined as no flow using Neumann conditions.
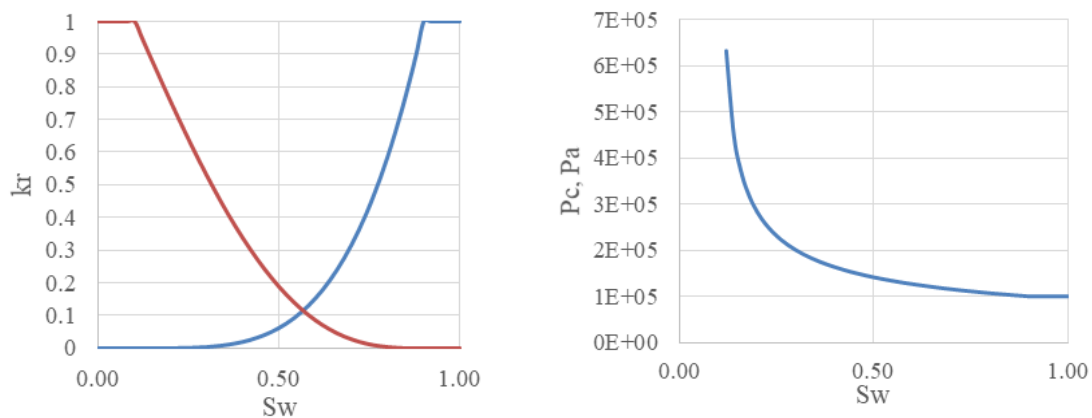
The development strategy of the model represents a constant injection but production after 2 years of the operation. The production well is placed on the crest of the structure, whereas the injection well position varies along the north flank of the dome (Figure 4-1).

After evaluation of the sensitivity analyses, the optimal parameters are selected for the base case scenario as follows:

- distance between wells: 350 m
- total injection rate: 15 moles/s
- injection gas composition: 50% N_2, 40% H_2, 10% CO_2
- total production rate: 13 moles/s
- simulation period: 30 years
- microbial kinetic parameters: Table 4-3

The model with the specified parameters is used as a base case and compared with all cases of sensitivity analysis. In total, 12 cases with different parameters are simulated (Table 4-2).

Table 4-2. Summary of different cases for sensitivity analysis

Parameter /case	Microbial kinetic parameters	Well spacing	Injection rate	Injection composition
1 (Base)	Base	350 m	15 mole/s	50% N_2, 40% H_2, 10% CO_2
2 (No Bio)	None	350 m	15 mole/s	50% N_2, 40% H_2, 10% CO_2
3	**Min**	350 m	15 mole/s	50% N_2, 40% H_2, 10% CO_2
4	**Max**	350 m	15 mole/s	50% N_2, 40% H_2, 10% CO_2
5	**Mean**	350 m	15 mole/s	50% N_2, 40% H_2, 10% CO_2
6	Base	350 m	**7 mole/s**	50% N_2, 40% H_2, 10% CO_2
7	Base	350 m	**30 mole/s**	50% N_2, 40% H_2, 10% CO_2
8	Base	**200 m**	15 mole/s	50% N_2, 40% H_2, 10% CO_2
9	Base	**600 m**	15 mole/s	50% N_2, 40% H_2, 10% CO_2
10	Base	350 m	15 mole/s	**0% N_2, 80% H_2, 20% CO_2**
11	Base	350 m	15 mole/s	**75% N_2, 20% H_2, 5% CO_2**
12	Base	350 m	15 mole/s	**90% N_2, 8% H_2, 2% CO_2**

Instead of using the mean values of microbial kinetic parameters as in Hagemann, 2018, the parameters for the base case are shown in Table 4-3. The microbial kinetics parameters are modified in a way to have sufficient methane in the produced gas. The used parameters in this thesis yield faster conversion rate of the injected gases.

Table 4-3. Microbial kinetic parameters used in the simulations

Parameters/ case	Mean	Min	Max	Base
$\psi_{m,max}^{growth}$ [1/s]	1.5e-5	1.505e-6	3.0e-5	3.0e-5
ψ_m^{decay} [1/s]	2.3e-6	2.3e-6	2.3e-6	2.3e-6
$\alpha_{m,H2}$ [mol/mol]	1.1e-5	3.24e-5	9e-10	1.1e-7
$\alpha_{m,CO2}$ [mol/mol]	3.2e-4	5.4e-4	2.3e-6	3.2e-5
Y [1/mol(H_2)]	1.7e12	1.1e13	7.7e10	2.5e11
n* [1/m^3]	6e10	6e10	6e10	6e10

The mentioned operational parameters for the base case ensure the arrival of CH_4 after 2 years of injection for the specified model's domain. The production rate is smaller than the injection rate due to stoichiometric relation of the methanogenic reaction. Where for 5 moles of gaseous reactants, there is only 1 mole of the gaseous product. The injection volume shrinks during methanation process, and the production volume must be lower than injection volume. Thus, the reduced production rate can ensure constant reservoir pressure.

After a couple of years of the operation, the hydrogen and methanogenic bacteria are distributed in the reservoir with a similar pattern. The microbial population is purely controlled by the distribution of the nutrients. The higher concentrations of the nutrients cause the high density of the microorganisms. For the base case, the methane concentration in the production well is around 9% after 30 years of operation. There is no CO_2 production due to conversion along the flow path. However, there is a small fraction of hydrogen in the produced gas which is not converted fully during the flow from the injector to the producer (Figure 4-3). The arrived hydrogen indicates that either the design of the wells or injection rates are not optimal. The pressure remains relatively constant due to the lower production rate over the injection rate.
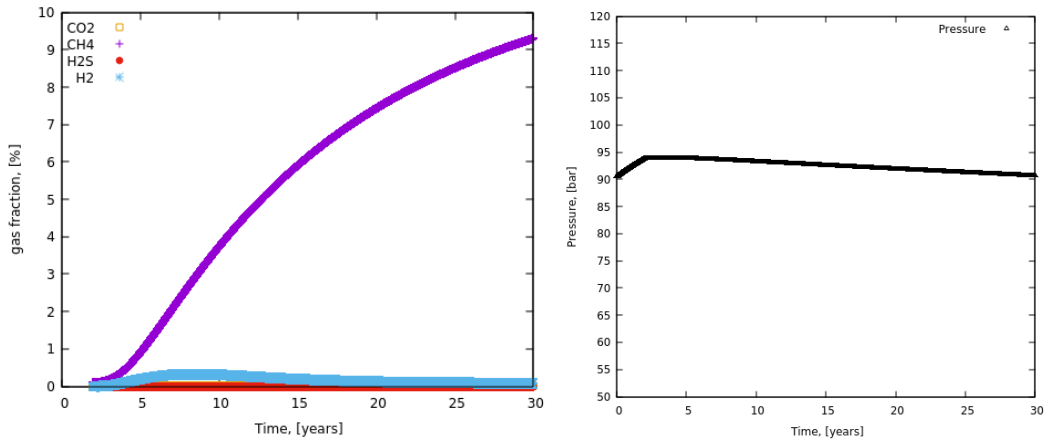
Figure 4-3. Composition of the produced gas without nitrogen (left) and the average reservoir pressure (right). Only methanogenic microorganisms are active (base case).

In the case when the reactions are disabled the hydrogen can propagate to the whole reservoir because there is no consumption of it. That is why after 30 years of simulation, the hydrogen is distributed in the whole reservoir. And the composition of the produced gas is different. Since there are no methanogenic archaea anymore, there is no production of the methane. All produced gas composition is controlled by the initial and injected gas mixing. Accordingly, the composition of the produced gas predominately consists of nitrogen. The rest of the produced gas consists of hydrogen and carbon dioxide that is injected into the reservoir.

When the reactions are disabled there is no shrinkage of the injected gas volume. For the same injection and production rate as for the base case, the pressure for this case increases which is caused by dominating injection rate over production rate (Figure 4-4).
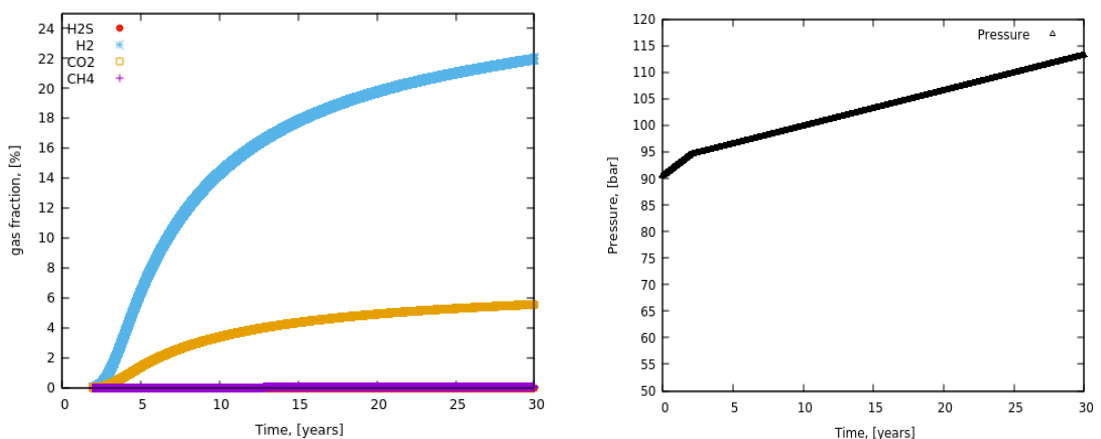

Figure 4-4. Composition of the produced gas without nitrogen (left) and the average reservoir pressure (right). No microbes are active.

4.1.3 Sensitivity analysis

For the sensitivity analysis, several cases are simulated. In the first part of the sensitivity analysis, the influence of the microbial kinetic parameters is analysed and discussed. It is followed by sensitivity analysis based on different operational parameters, namely well spacing, injection rate and composition. Based on that, the optimal well spacing, injection rate and composition are purposed. The parameters used for every scenario are shown in Table 4-2 and Table 4-3.

4.1.3.1 Sensitivity analysis based on microbial kinetic parameters

In the work of (Hagemann, 2018), the kinetic parameters for methanogenic archaea are gathered from different sources. The range of every kinetic parameter is in order of few magnitudes. Hence, the effect of such uncertainty can be high and must be analysed.

Sensitivity analysis is performed to study the influence of the kinetic parameters to microbial population dynamics and methane yield. In the beginning, the microbial kinetics parameters are chosen in a way to have a minimum conversion (case 3). The methane fraction in the produced gas is less than 0.1%. At the same time, the produced gas composition is similar to the injection composition (Figure 4-5). After the start of the production, the reservoir pressure increases from 95 bar till 113 bar. The case with mean values (case 5) the behaviour of the pressure and the produced composition are similar to the case with minimum values. In total, the pressure behaviour and the produced composition are similar for the cases with no microbial reactions (case 2), minimum values (case 3) and mean values (case 5) of the microbial kinetic parameters.
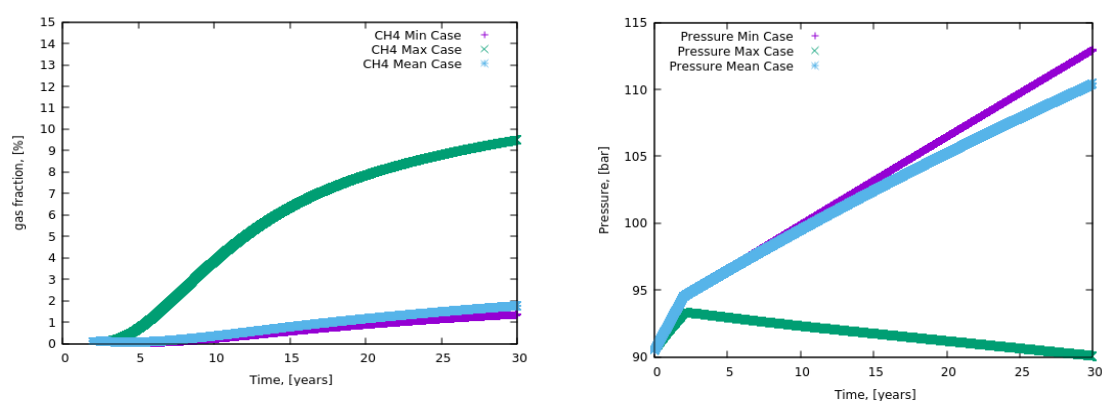
Figure 4-5. Minimum and maximum reaction

In the case of maximum methanogenesis (case 4), the hydrogen and carbon dioxide fraction is less than 0.1%. It is explained by the fact that all nutrients are almost immediately converted after being injected. Maximum reaction rates can cause high methane concentration as well as the increased water saturation. One could expect that excessive water can become mobile because the residual water saturation is exceeded. However, the simulation results show that

the mobile water does not reach a region drained by the production well (Figure 4-6). Due to the high mobility ratio between gas and water, the displacement efficiency of water by gas phase is low. Accordingly, the water blocking is not expected. In addition to that, the microbial conversion efficiency is high enough to have a limited microbial distribution. This effect is controlled by yield coefficient Y which defines the amount of newly grown microorganisms per 1 mole of the converted methane.

Figure 4-6. Water saturation after 30 years of simulation for the case with maximum methanogenesis
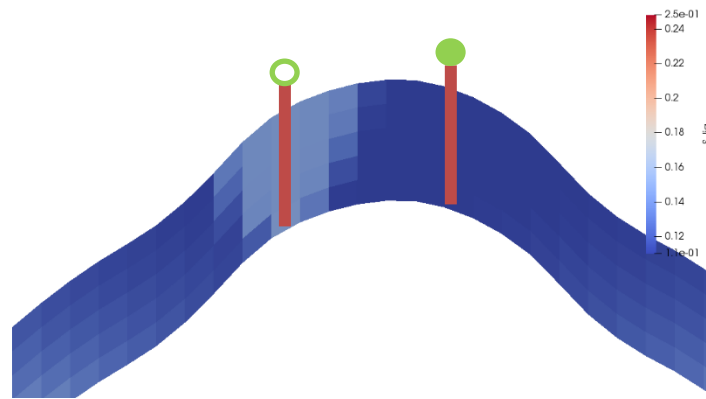
The situation with lower microbial activity and larger microbial distribution may be different. Due to lower microbial activity, the microbial distribution is expected to be wider due to the extended nutrients distribution. Thus, the water as a product of the reaction can appear in the area drained by the producer. However, for the field scale simulation in this thesis, water production is not observed.

This sensitivity analysis shows that the microbial kinetic parameters have a huge impact on the results of the methanation process, but remain poorly studied. By using the extreme values, one can expect the behaviour of instant conversion of the nutrients or almost no nutrients consumption at all for the 30 years of operation. Thus, the uncertainty in the microbial kinetic parameters has to be reduced by conducting laboratory experiments for the specific site conditions. This could ensure a more accurate prediction of the microbial distribution and, hence, the precise amount of the produced methane in the reservoir.

4.1.3.2 Design of UMR operation

Based on the experience in the past, there are several cases when the injected gas is converted into methane and the visible changes in the produced gas are recorded. That is why the potential of the bio-methanation remains and the microbial activity is only a matter of the reservoirs with favourable conditions for the microbial growth and conversion. In this section, the microbial kinetic parameters are used the same as for the base case (Table 4-3). Here it is necessary to answer the question about optimal operational parameters that provide limited production of nutrients and maximum concentration of methane in the produced gas. An optimized

methanation process can be described by the fact that all injected hydrogen and carbon dioxide are converted before reaching a production well.

The UMR in the reservoir can be characterized by 3 zones (Figure 4-7). The first zone, which is around the injection well is characterized by the gas composition close to the injected gas composition. The second zone consists of injected nutrients, initial reservoir gas and the methane as the product of the methanation. The last zone is specified as the zone with no available nutrients.
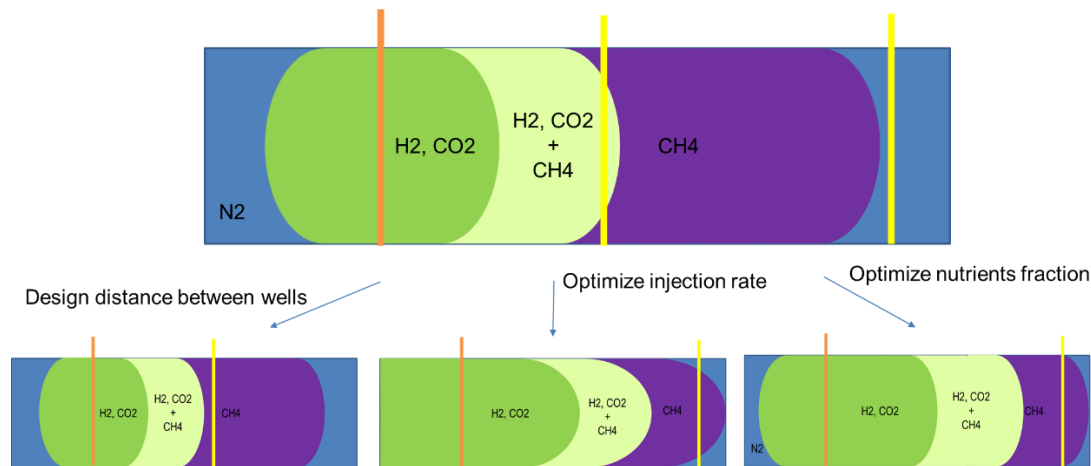

Figure 4-7. Designing the underground methanation process

The most optimal way is to produce the gas from the 3rd zone where there are no initially injected nutrients are present. Furthermore, the production well should be placed as close as possible to the beginning of the 3rd zone. From one side, that will ensure the shortest time of methane front to reach the production. On the other side, the concentration of methane in the product gas can be the highest because it will be less mixed with the initial reservoir gas.

The injection of total gas with 40 moles/s shows production of H_2 and CO_2. Injection with a rate lower than 15 moles/s (40% H_2, 10% CO_2) indicates no production of the nutrients; therefore it can be considered as the optimal rate for such case (Figure 4-8). In the case of the fixed injection rate, which is 15 moles/s (40% H_2, 10% CO_2), the simulation results show that the optimal distance between the wells is 350m. For the cases with the shorter distances, there is a production of nutrients and considering longer distances, it takes more time for methane to reach the production well (Figure 4-9). Comparing different injection compositions, the injection of 20% of H_2 and 5% of CO_2 shows relatively low hydrogen fraction in the produced gas as well as low methane concentration in the produced gas. Simultaneously, the injection of 80% hydrogen shows the highest methane concentration but a high concentration of the hydrogen. Thus, the case with 40% hydrogen injection is considered as the optimal due to moderate methane concentration and low hydrogen concentration in the produced gas.
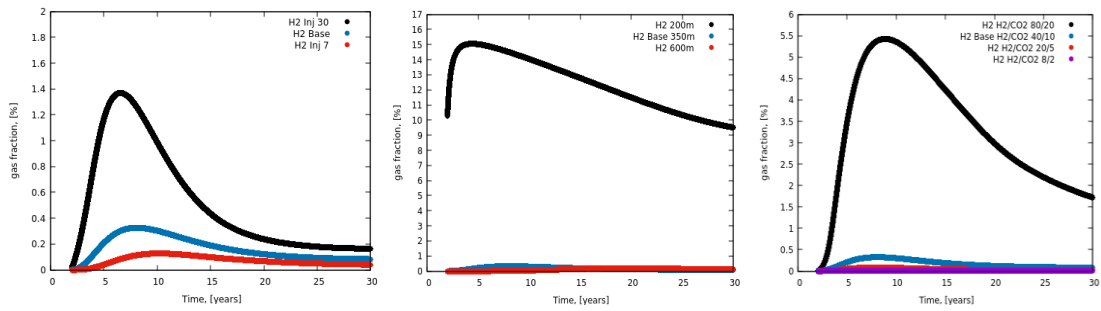
Figure 4-8. The hydrogen concentration in the produced gas. Sensitivity analysis based on different injection rates, distances between wells, and the different ratios between H_2 and CO_2
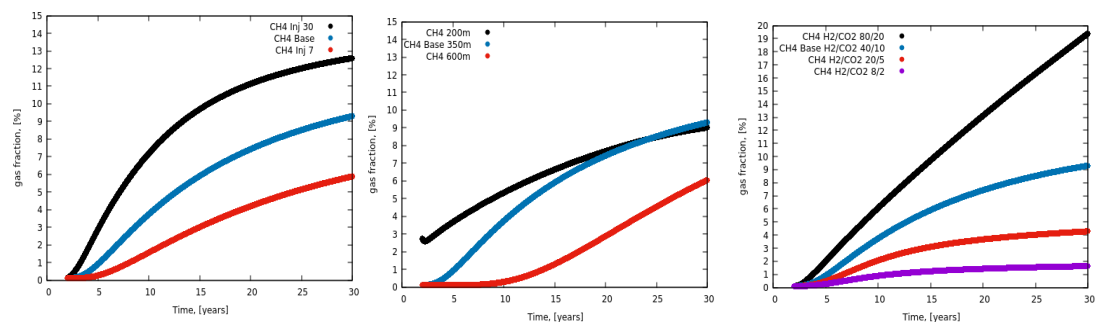

Figure 4-9. Methane concentration in the produced gas. Sensitivity analysis based on different injection rates, distances between wells, and the different ratios between H_2 and CO_2

This sensitivity analysis shows how the operational parameters can be varied to optimize the underground methanation process. While knowing constraints of the storage site one can vary 3 parameters to convert all the injected gas and have high methane yield and pureness. In the case of the new development of the UGS facility, one can design the well spacing to ensure the conversion of a certain amount of the hydrogen supply. However, for the case of depleted gas fields, or pre-designed UGS facility the injection rate or composition has to be optimised. Which brings some limitations to the hydrogen generation plants or the pureness of the produced methane.

Such designing of the UMR is only applicable for the storages with different than methane compositions. However, during the storage in the depleted gas reservoir, there is only need for excluding the hydrogen and carbon dioxide production. That is why for the case of a reservoir filled with methane, the long distance between the wells, low injection rate and low fraction of nutrients can assure no nutrients production.

4.2   Field-scale simulation

Here is the subchapter of results from a field-scale sector grid. Where the potential of bio-methanation discussed assuming the 40 MW wind park power supply.

4.2.1 Reservoir characterization and geomodelling

The Middle Buntsandstein as one of the most common reservoir layers in Germany is chosen for the field scale conceptual model. The Middle Buntsandstein consists of Volpriehausen, Detfurth, Hardegsen and Solling formations (Table 4-4). Units of fluvial to lacustrine sediments and aeolian sediments compose the Middle Bundsandstein. The sediments transport is presented by the braided rivers and wind with the general transport towards the North (Gaupp et al., 1998).

Table 4-4. *Stratigraphic subdivisions of the Middle Buntsandstein Group in the German Basins*

Group	Formation
Middle Buntsandstein (sm)	Solling Fm (smS)
	Hardegsen Fm (smH)
	Detfurth Fm (smD)
	Volpriehausen Fm (smV)

In this work, the correlation between reservoir properties and depositional environments are assumed. Thus, the facies types correspond to sediments of certain depositional environments. In Table 4-5 the mean reservoir properties of defined facies are shown. These properties for specified facies are used further for geomodelling.

Table 4-5. *Reservoir properties of defined facies (Beyer et al., 2014)*

depositional environment	sandflat	fluvial	aeolian
deposits	sand/mud sheet	channel	desert sand
main formation	smV, smD, smH	smS, smH	smV, smD, smH
the ratio of sandstone to mudstone	moderate (2:1)	low (10:1)	very low (50:1)
sandstone thickness	decimetres	metres	centimetres to decimetres
mean grain size	0.22 mm	0.23 mm	0.44 mm
mean carbonate cement content	2.10%	4.80%	2.70%
mean sulphate cement content	2.70%	5.00%	6.70%
mean blocky cement content	9.50%	14.50%	13.60%
mean clay content	7.90%	2.00%	3.10%
special features	various characteristics	less clay	coarse grains
mean porosity	13.00%	11.90%	13.40%
mean permeability	27.2 mD	57.8 mD	108.7 mD

For the model, a synthetic reservoir structure is used by assuming the closure of 150m. The grid cells have dimensions of 50x50x5 m.

For Volpriehausen and Detfurth formations, a vertical proportion between the floodplain and aeolian facies is taken from (Baena, 2011). The parameters for fluvial channels are taken from the Waimakariri braided river analogy. The channel amplitude is specified between 50 and 300 m, the wavelength is between 300 and 1000m. The channels width is similar for all formations and equals to 5-20 m. The mean depths of fluvial channels are considered from Baena, 2011. The channel depths vary for each formation as follows:

- Solling formation: between 3 and 11 m
- Hardegsen formation: between 11 and 14 m
- Detfurth formation: between 10 and 12 m
- Volpriehausen formation: between 4 and 31 m

For petrophysical modelling, the minimum, mean and maximum values of the properties are used from (Beyer et al., 2014). The reservoir properties are shown in Table 4-5. For spatial distribution, the typical variograms for certain depositional environments are taken from (Zhang et al., 2005). The major direction of the variograms is north, which is consistent with the general transport of sediments.

For some German reservoirs, The Solling and Hardegsen formations are characterized as a poor reservoir. Sometimes these formations are developed even individually due to low hydrodynamic connectivity between formations. Subsequently, these two formations are excluded from simulation, and only Detfurth and Volpriehausen formations are considered for the simulation. To reduce computation time, only a sector model is selected to avoid excessive coarsening of grid cells. This implies that the sector model can be a good representation of the reservoir flow regime. The final porosity distribution is shown in Figure 4-10.
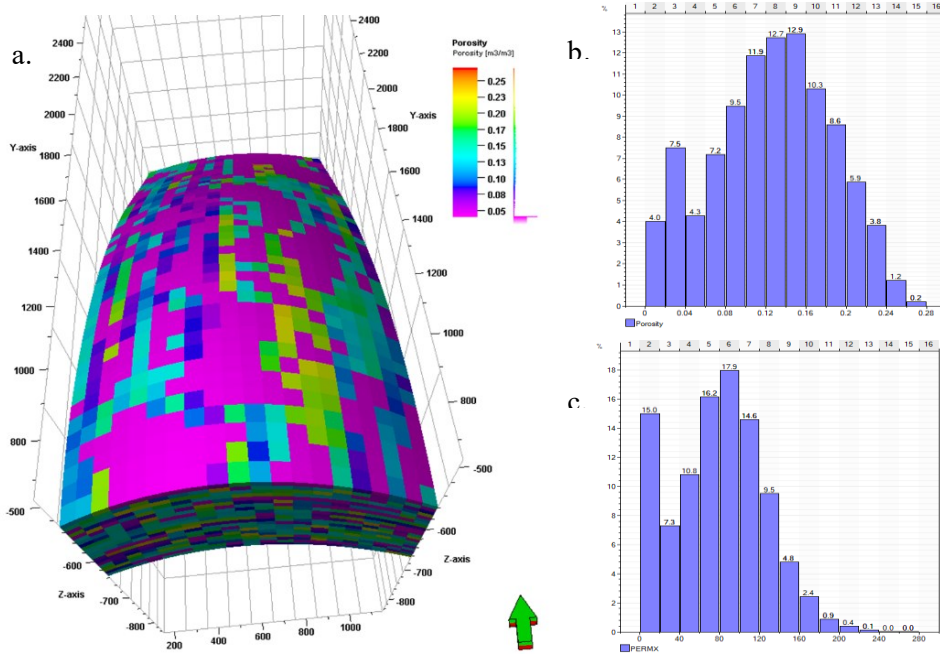
Figure 4-10. 3D model of porosity distribution (a), histogram plot of porosity (b) and permeability (c) distributions for reservoir facies of Detfurth and Volpriehausen formations

4.2.2 Numerical simulation

The saturation and pressure of the model are assigned at the initialization stage in DuMux. The gas water contact (GWC) is at the 720m (true vertical depth) and the pressure at the GWC is equal to 72 bar. The saturation above GWC is at the residual water saturation 11%. The initial gas composition is 100 % of methane (Table 4-6). The properties of fluids and components, rock-fluid interaction are considered the same as in the previous homogeneous model. All boundaries are defined as no flow using Neumann conditions.

Table 4-6. Initial parameters of the field-scale model

Parameter	Value	Unit
GWC	720	m (TVD)
Pressure @ GWC	72	Bar
Temperature	40	^{o}C
GIIP	2.25E+07	rm^3
Number of grid cells	20164	-
Initial composition:		
CH_4	100	%

Based on the upcoming „Energiepark Bad Lauchstädt" project, for the simulation process, it is assumed the same power supply which is 40 MW coming from the wind park (Kaiser, 2019). The typical capacity factor for land wind plants in Germany is 30% (BWE, 2020), thus the annual energy production from such wind plant can be around 105 GWh. According to (Bertuccioli et al., 2014), the energy cost of PEM electrolyser is equal to 48 kWh per 1 kg of hydrogen. Which indicates the annual potential of 2.2E+06 kg of hydrogen production or 35 moles/s of hydrogen (Table 4-7).

Table 4-7. The hydrogen production from the 40 MW wind park

Parameter	Value
Wind park Power	40 MW
Capacity factor	30%
Energy input	48 kWh/kg H_2
Hydrogen production	2.2E+06 kg/year
Injection rate	2822 sm^3/h 35 moles/s

For the simulation scenario, the injection gas composition is 80% - H_2, and 20% - CO_2. Thus, the total injection rate which is used in the following simulation is 44 moles/s. For the sake of constant reservoir pressure, the production rate is 5 times smaller than the injection rate. This production rate reduction is a possible approach to honour the stoichiometric relation of the methanogenic reaction. The microbial kinetic parameters are used the same as for the base case of the homogeneous model.

In the previous section, the necessity of the optimal design of UMR is discussed. Here, the hydrogen rate is fixed, consequently, only the well spacing can be varied. One concern during the operation period is related to the elimination of H_2 and CO_2 production. Hence, the injector and producer must be adequately placed far away to allow conversion of the injected gases by microbial. Based on the results from the previous section, the well spacing of 750 m is a reasonable distance.

In this case, the simulation of underground methanation process in a reservoir filled with methane is performed. The model mimics the constant injection during all 30 years of operation. The fluid is injected at the top of the Detfurth formation with the perforated zone of 20 metres below the top. The production starts after 2 years of gas injection when the reservoir pressure reaches 75 bars. The production interval has the same 20 m of perforation bellow the top of the Detfurth formation. The production well is located on the crest of the structure while the injection well is placed on the northern flank (Figure 4-12). The wells are positioned in a way

to honour the connectivity caused by South-North paleo transport of the sediments. Since the reservoir model is initialized with methane, one can hardly distinguish between the original methane in place and methane as a product of the methanogenic reaction. Despite the previous simulation approach in the homogenous model, the production from a methane reservoir can be started regardless of reaching the injected/converted gas front to the producer. This is because at the first place the initial methane is produced and on the later stages production incorporates the converted methane as well. Nevertheless, the reservoir pressure must fulfil the requirements of the production planning. Here it is assumed, that the average reservoir pressure must be beyond 75 bar overproduction period.

At the beginning of the operation, the shape of the injected gas is semi-circular which is controlled by a radial pressure gradient caused by the injection. On later stages, the shape of the gas mixture spreads more in the longitudinal direction due to the elongated structure and heterogeneity of the reservoir (Figure 4-11).
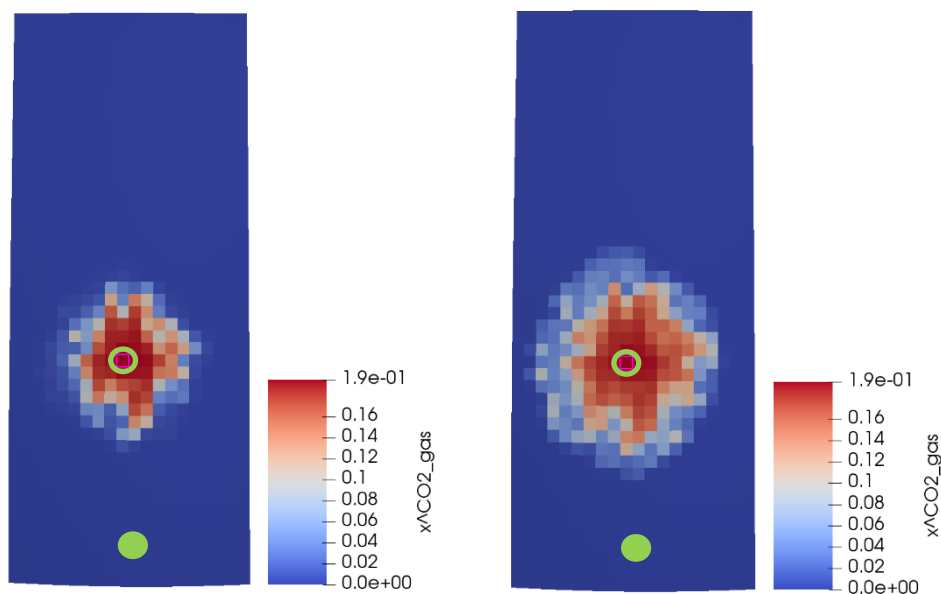

Figure 4-11. The CO₂ concentration in the reservoir after 3 years (left) and 18 years (right. Wells are indicated with squares.

Hydrogen density in the reservoir conditions is lower than the density of the initial reservoir gas (methane). However, the injected gas mixture of hydrogen and carbon dioxide have comparable densities with the methane. That is why the lateral spreading of the injected gas along the cap rock and gravity override is not significant. Lateral spreading of the gas is predominant in the aquifer due to the high contrast between the water and hydrogen densities. After 30 years of hydrogen and carbon dioxide co-injection, it can be seen that the initial gas spreads laterally along the cap rock while displacing the water from the aquifer (Figure 4-12). Thus, the area near the aquifer requires a closer look during the operation because it can lead

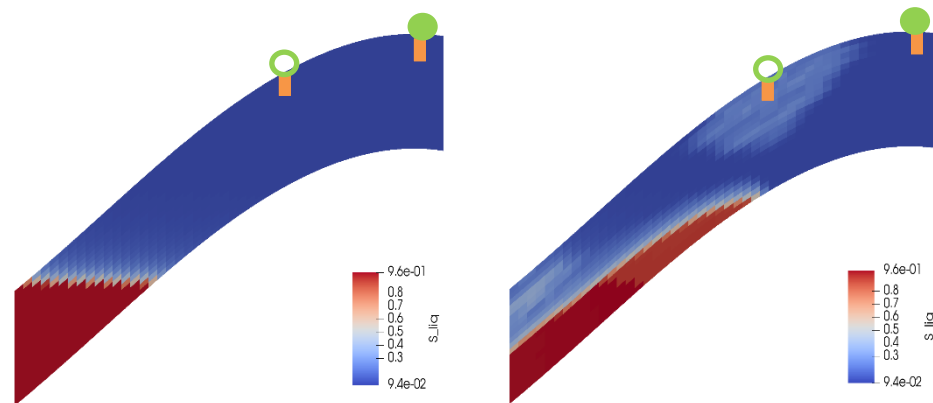to the spreading of the gas beyond the spill point as it is discussed in the literature review section.

Figure 4-12. Water saturation at the beginning (left) and after 30 years of the operation (right)

The simulation result shows that there is a production of H_2 after 8 years due to reaching of injected gas front to the producer. However, the fraction of the hydrogen in the produced gas only reaches 1.5% after 30 years (Figure 4-13). That means that the rest of the gas is successfully converted to methane. Moreover, there is no significant change in the hydrogen and carbon dioxide distribution after 6 years of the operation (Figure 4-14). The reservoir pressure after 10 years is stabilized at the level of 78 bars till the end of the withdrawal period. As soon as the pressure reaches a constant level, it can be stated that the injected volume is equal to the produced volume. As discussed earlier, the production rate is considered 5 times less than the injection rate due to the stoichiometric relation of the reaction. Such equilibrium can reveal that most of the injected hydrogen is apparently converted to the methane. It can justify the constant reservoir pressure for misbalanced injection and production.
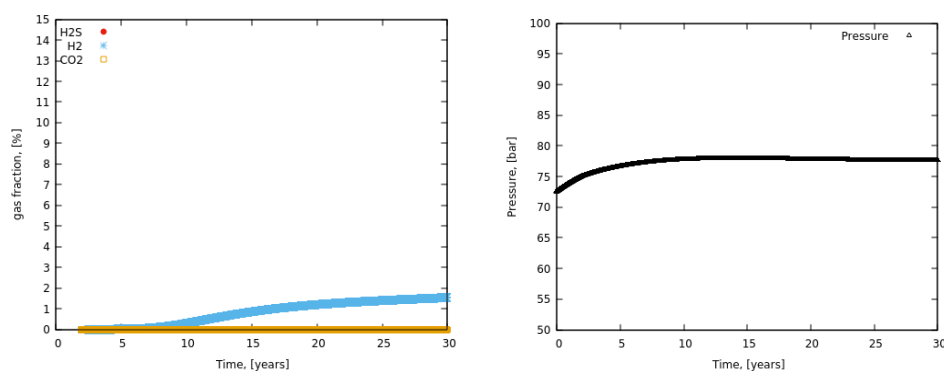
Figure 4-13. The gas composition of the produced gas (left) and reservoir pressure (right)

The 4:1 ratio between the hydrogen and carbon dioxide should reveal the full conversion of the nutrients in the reservoir filled with methane. However, the results of the gas composition show 1.5% of hydrogen production (Figure 4-13). According to (Wilke & Lee, 1955) the hydrogen-methane molecular diffusion is 4 times higher than the one for the carbon dioxide-methane of

the binary mixture at the standard conditions. At the same time, the hydrogen solubility is lower than for carbon dioxide. Knowing that it could be assumed that the gaseous hydrogen diffuses into the reservoir without fully dissolving or transforming at the early stages of the operation. However, carbon dioxide is not transported due to lower diffusivity and higher solubility. At later stages of operation, the microbial community is developed enough to consume all the injected nutrients. Consequently, the hydrogen is not transported into the reservoir anymore. And the low concentration of the hydrogen at the later stages can be produced until depletion of the diffused hydrogen relict. At the same time, the diffused hydrogen cannot be converted into methane due to the absence of the carbon dioxide in the reservoir. Thus, for the case of initial presence of carbon dioxide in the reservoir one can assume no production of the diffused hydrogen. Because the presence of nutrients and microorganisms in the reservoir would initiate the methanogenesis and consumption of the nutrients. An option to mitigate the hydrogen production can be the prior injection of the carbon dioxide into the reservoir before the injection of the gas mixture.
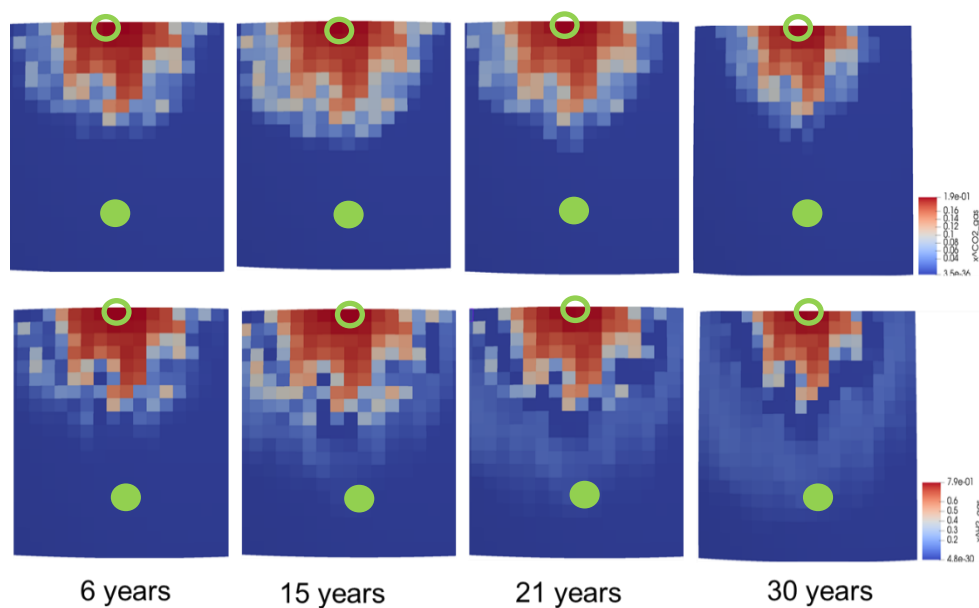

Figure 4-14. Carbon dioxide concentration (upper row) and hydrogen concentration (lower row) distributions

The increasing of the water saturation from 11% to 28% is observed in the area near to the injection well (Figure 4-15). The simulation results show that for this case the mobile water cannot reach to the region around the production well. Meanwhile, the area with increased water saturation is limited with the microbial community presence, which is also present mostly around the injection well (Figure 4-15). As a result, there is no evidence of excessive water production after 30 years of operation for both cases.
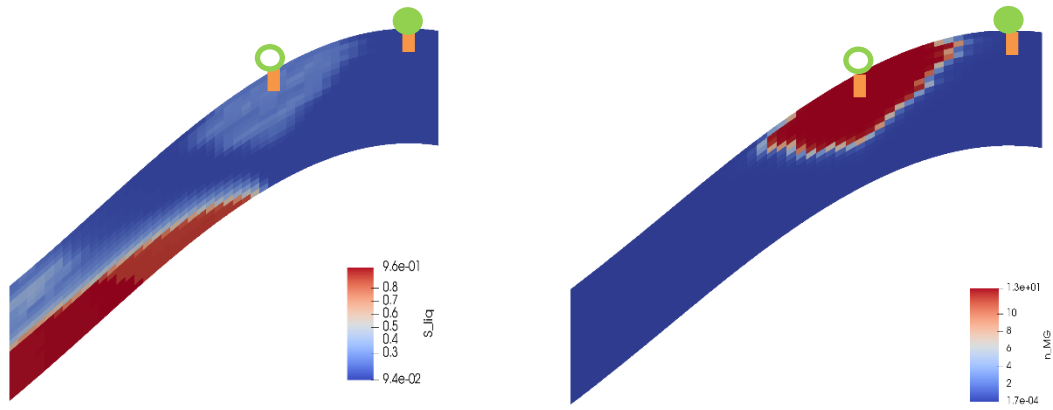
Figure 4-15. The water saturation (left) and the dimensionless density of methanogenic archaea concentration (right) after 30 years of the operation

After 30 years of production, the amount of hydrogen left in the reservoir is equal to 2.71E+09 moles. Considering the injection rate of 35 mole/s during this time, the cumulative injected amount of hydrogen is equal to 3.3E+10 moles, where 3.04E+10 moles of hydrogen has been converted into 7.6E+9 moles of methane that maintain the pressure of 78 bars till the end of the operation.

Chapter 5

Conclusion

5.1   Summary

Based on the performed sensitivities, well spacing, injection rate and composition are purposed as design parameters for the underground bio-methanation projects. For the case of reuse of abandoned gas/oil field, underground gas storage, one can adjust the injection rate or composition to ensure the full conversion of the injected hydrogen and carbon dioxide. For the case with the well planning and fixed hydrogen supply, the well spacing as the main design parameter should be considered.

During the underground methanation, in most of the cases, the water blocking is not an issue due to low incremental water saturation caused by microbial metabolism.

During the development of the reservoir without initial carbon dioxide, the pre-injection of carbon dioxide can be an option for mitigating the hydrogen production caused by its faster diffusion than for carbon dioxide.

For the case of 40 MW PEM electrolyser the produced hydrogen can be successfully converted in the reservoir with a gas volume of $2.25E+07\,rm^3$. The long well spacing is a good criterion for the conversion process in the reservoir predominately filled with methane.

5.2   Future Work

For designing a field-scale operation the knowledge of the microbial kinetic parameters are essential. For the current state, the knowledge about these parameters values is small. In critical cases, it can cause no methane for 30 years of the operation.

The work presents the first results of underground bio-methanation in the field-scale reservoir. However, it should be revised after the appearance of the lab experiments of microbial kinetic parameters for the specific reservoir conditions.

<div align="right">

Chapter 6

</div>

References

Ahmed, T. H. (2010). *Reservoir engineering handbook* (4th ed.). Gulf Professional Pub.

Ananthanarayan, R., & Paniker, C. J. (2008). *Ananthanarayan and Paniker's textbook of microbiology* (7th ed., repr.). Orient Longman Private Ltd.

Baena, J. (2011). *3d-facies and reservoir modelling of the Buntsandstein reservoirs of the northwestern Thuringian Syncline* [, Jena]. RIS. https://www.db-thueringen.de/receive/dbt_mods_00019423

Bauer, S. (2017). *Underground Sun.Storage Final Report*. https://www.underground-sun-storage.at

Bertuccioli, L., Chan, A., Hart, D., Lehner, F., Madden, B., & Standen, E. (2014). Study on development of water electrolysis in the EU. *Fuel Cells and Hydrogen Joint Undertaking*.

Beyer, D., Kunkel, C., Aehnelt, M., Pudlo, D., Voigt, T., Nover, G., & Gaupp, R. (2014). Influence of depositional environment and diagenesis on petrophysical properties of clastic sediments (Buntsandstein of the Thuringian Syncline, Central Germany). *Zeitschrift Der Deutschen Gesellschaft Für Geowissenschaften*, *165*(3), 345–365. https://doi.org/10.1127/1860-1804/2014/0072

Bielinski, A. (2007). *Numerical simulation of CO2 sequestration in geological formations.* https://doi.org/10.18419/opus-252

BWE. (2020). *BWE Industry Report - Wind Industry in Germany.*

Corey, R. H. B. a. A. T. (1964). Hydraulic Properties of Porous Media and Their Relation to Drainage Design. *Transactions of the ASAE*, *7*(1), 26–28. https://doi.org/10.13031/2013.40684

Das, L. M. (2016). Hydrogen-fueled internal combustion engines. In *Compendium of Hydrogen Energy* (pp. 177–217). Elsevier. https://doi.org/10.1016/B978-1-78242-363-8.00007-4

Feldmann, F., Hagemann, B., Ganzer, L., & Panfilov, M. (2016). Numerical simulation of hydrodynamic and gas mixing processes in underground hydrogen storages. *Environmental Earth Sciences*, *75*(16), 103. https://doi.org/10.1007/s12665-016-5948-z

Fick, A. (1855). Ueber Diffusion. *Annalen Der Physik Und Chemie*, *170*(1), 59–86. https://doi.org/10.1002/andp.18551700105

Flemisch, B., Darcis, M., Erbertseder, K., Faigle, B., Lauser, A., Mosthaf, K., Müthing, S., Nuske, P., Tatomir, A., Wolff, M., & Helmig, R. (2011). DuMux: DUNE for multi-{phase,component,scale,physics,…} flow and transport in porous media. *Advances in Water Resources*, *34*(9), 1102–1112. https://doi.org/10.1016/j.advwatres.2011.03.007

Gaupp, R., Voigt, T., Lützner, H., Müller, H., & Föhlisch, K. (1998). Stratigraphy and sedimentological evolution of Lower and Middle Triassic deposits in the SE part of the Germanic Triassic Basin, 99–120.

Hagemann, B., Rasoulzadeh, M., Panfilov, M., Ganzer, L., & Reitenbach, V. (Eds.) (2014). *ECMOR XIV - 14th European Conference on the Mathematics of Oil Recovery*. *Proceedings*. EAGE Publications BV Netherlands.

Hagemann, B., Rasoulzadeh, M., Panfilov, M., Ganzer, L., & Reitenbach, V. (2016). Hydrogenization of underground storage of natural gas. *Computational Geosciences*, *20*(3), 595–606. https://doi.org/10.1007/s10596-015-9515-6

Hagemann, B. (2018). *Numerical and Analytical Modeling of Gas Mixing and Bio-Reactive Transport during Underground Hydrogen Storage. Schriftenreihe des Energie-Forschungszentrums Niedersachsen (EFZN): v. 50*. Cuvillier Verlag.

Hassannayebi, N. (2019). *An assessment of underground hydrogen storage: Transport, geochemistry, and bioactivity* [Ph.D. thesis], Montanuniversität Leoben.

Ho, C. K., & Webb, S. W. (2006). *Gas Transport in Porous Media* (Vol. 20). Springer Netherlands. https://doi.org/10.1007/1-4020-3962-X

Hogeweg, S., Strobel, G., & Hagemann, B. (2020). Hogeweg 2020. Simulation of Underground Microbiological Methanation in a Conceptional Well Doublet System 4, *2/2020*. DOI 10.19225/200202

Kaiser, P. (2019). *„Energiepark Bad Lauchstädt" - Das mitteldeutsche Power-to-gas/H2-Reallabor der Energiewende*. 12. Sächsisches Fachsymposium ENERGIE 2019, Dresden.

Lalli, C. M., & Parsons, T. R. (1997). *Biological oceanography: An introduction* (2nd ed.). *Open University oceanography series*. Butterworth Heinemann.

Maier, R. M., Pepper, I. L., & Gerba, C. P. (2009). *Environmental microbiology* (2nd ed.). Elsevier/Academic Press.

Megee, R. D., Drake, J. F., Fredrickson, A. G., & Tsuchiya, H. M. (1972). Studies in intermicrobial symbiosis. Saccharomyces cerevisiae and Lactobacillus casei. *Canadian Journal of Microbiology*, *18*(11), 1733–1742. https://doi.org/10.1139/m72-269

Merriam-Webster. (2020). *Merriam-Webster.com dictionary*. https://www.merriam-webster.com/dictionary/pleuston

Meyers, R. A. (2002). *Encyclopedia of physical science and technology* (3rd ed.). Academic.

Mohanta, T., Dutta, D., & Goel, S. (2017). Fundamentals of Microbiology. In S. Goel (Ed.), *Advances in Solid and Hazardous Waste Management* (Vol. 10, pp. 301–321). Springer International Publishing. https://doi.org/10.1007/978-3-319-57076-1_15

Oldenburg, C. M. (2003). Carbon Dioxide as Cushion Gas for Natural Gas Storage. *Energy & Fuels*, *17*(1), 240–246. https://doi.org/10.1021/ef020162b

Panfilov, M. (2016). Underground and pipeline hydrogen storage. In *Compendium of Hydrogen Energy* (pp. 91–115). Elsevier. https://doi.org/10.1016/B978-1-78242-362-1.00004-3

Panfilov, M. B. (2018). *Physicochemical fluid dynamics in porous media: Applications in petroleum geosciences and petroleum engineering / Mikhail Panfilov* (1st). Wiley-VCH.

Parker, N., Schneegurt, M., Tu, A.-H. T., Forster, B. M., & Lister, P. (2018). *Microbiology* (Revision MB-2016-002(05/18)-BB). OpenStax.

Pfeiffer, C., Bach, M., Bauer, T., Campos da Ponte, J., Schömig, E., & Gründemann, D. (2015). Knockout of the ergothioneine transporter ETT in zebrafish results in increased 8-oxoguanine levels. *Free Radical Biology & Medicine*, *83*, 178–185. https://doi.org/10.1016/j.freeradbiomed.2015.02.026

Poling, B. E., Prausnitz, J. M., & O'Connell, J. P. (2000). *The properties of gases and liquids* (5th ed.). McGraw-Hill.

Reitenbach, V., Ganzer, L., Albrecht, D., & Hagemann, B. (2015). Influence of added hydrogen on underground gas storage: a review of key issues. *Environmental Earth Sciences*, *73*(11), 6927–6937. https://doi.org/10.1007/s12665-015-4176-2

Sainz-Garcia, A., Abarca, E., Rubi, V., & Grandia, F. (2017). Assessment of feasible strategies for seasonal underground hydrogen storage in a saline aquifer. *International Journal of Hydrogen Energy*, *42*(26), 16657–16666. https://doi.org/10.1016/j.ijhydene.2017.05.076

Strobel, G., Hagemann, B., Huppertz, T. M., & Ganzer, L. (2020). Underground bio-methanation: Concept and potential. *Renewable and Sustainable Energy Reviews*, *123*, 109747. https://doi.org/10.1016/j.rser.2020.109747

Tek, M. R. (1989). *Underground Storage of Natural Gas: Theory and Practice* (N). Springer Netherlands.

Wilke, C. R., & Lee, C. Y. (1955). Estimation of Diffusion Coefficients for Gases and Vapors. *Industrial & Engineering Chemistry*, *47*(6), 1253–1257. https://doi.org/10.1021/ie50546a056

Zhang, Y., Person, M., Paola, C., Gable, C. W., Wen, X.-H., & Davis, J. M. (2005). Geostatistical analysis of an experimental stratigraphy. *Water Resources Research*, *41*(11), 7. https://doi.org/10.1029/2004WR003756